UC Riverside

UC Riverside Electronic Theses and Dissertations

Title

Paper-Based Microfluidics: DNA Detection via Wicking Distances of Microsphere Aggregates and the Effects of Laser-Etching on Wicking Speeds in Paper Channels

Permalink

https://escholarship.org/uc/item/9zs5j2wn

Author

Kalish, Brent

Publication Date

2019

Peer reviewed|Thesis/dissertation

eScholarship.org Powered by the California Digital Library
University of California

UNIVERSITY OF CALIFORNIA
RIVERSIDE

Paper-Based Microfluidics: DNA Detection via Wicking Distances of Microsphere Aggregates and the Effects of Laser-Etching on Wicking Speeds in Paper Channels

A Dissertation submitted in partial satisfaction
of the requirements for the degree of

Doctor of Philosophy

in

Mechanical Engineering

by

Brent Nathaniel Kalish

December 2019

Dissertation Committee:
Dr. Hideaki Tsutsui, Chairperson
Dr. Masaru Rao
Dr. Bhargav Rallabandi

Copyright by
Brent Nathaniel Kalish
2019

The Dissertation of Brent Nathaniel Kalish is approved:

_____

_____

_____

Committee Chairperson

University of California, Riverside

ACKNOWLEDGMENTS

First and foremost, I would like to thank my advisor, Dr. Hideaki Tsutsui. I met Dr. Tsutsui in my final year of undergraduate studies and in the years since, he has provided the direction and support necessary for me to develop the skills I needed succeed in graduate school; both as a research and a teaching assistant. He taught me how to systematically investigate a hypothesis and to effectively communicate my findings to others both within the lab and to the wider scientific community. Without Dr. Tsutsui's guidance, I would not be who I am today.

I would also like to thank my fellow graduate student lab mates for their friendships over the years and for their aid in talking out difficult research problems. In particular I would like to thank Mr. Jianhou Zhang for all his work with me on the microsphere aggregation project, both as an undergraduate and now as a graduate student. The aggregate size study from chapter 3 was done by him.

I would like to thank Dr. Richard Echodu and Mr. Hilary Edema for their hospitality and instruction when I traveled to Uganda. I learned a great deal regarding viral detection in sweet potatoes and the design requirements for the microfluidic device I was designing.

I would also like to thank the following sources for their financial support during my graduate studies here at UCR: The Lung-Wen Tsai Memorial Design Award, the Department of Mechanical Engineering's Dissertation Year Award, and the Graduate Research Mentorship Program Fellowships. My research was also supported by a contract (UCR-14080823) to the University of California, Riverside from Gulu University through

the Bill & Melinda Gates Foundation's Program for Emerging Agricultural Research Leaders (OPP1112536) and by the National Science Foundation under Grant No. CBET-1606181. Electron microscopy was performed on a FEI NovaNanoSEM 450 in the Central Facility for Advanced Microscopy and Microanalysis (CFAMM) at UC Riverside.

Material from Chapter 4 will be published in an upcoming special issue of SLAS Technology in February of 2020 titled: "Flexible Analytical Devices for Point-of-Care Testing."

ABSTRACT OF THE DISSERTATION

Paper-Based Microfluidics: DNA Detection via Microsphere Aggregate Wicking Distances and the Effect of Laser-Etching on Wicking Speeds in Paper Channels

by

Brent Nathaniel Kalish

Doctor of Philosophy, Graduate Program in Mechanical Engineering
University of California, Riverside, December 2019
Dr. Hideaki Tsutsui, Chairperson

The development of patterning high-resolution microfluidic circuits onto cellulose paper in 2007 initiated widespread research into the use of the paper as a low-cost, easy-to-use alternative substrate over the glass and plastics of traditional microfluidics. Paper, as a porous hydrophilic material, naturally wicks fluid through itself, without the need for external pumps or power sources. The simplest paper-based devices are lateral flow devices, where liquid wicks in one direction along the paper strip. These are suitable for simple detection chemistries; however, for more complex reactions, devices that are more complicated are required, and this frequently entails the sequential delivery of different liquids or reagents to reaction zones. To achieve sequential delivery, one can manually deposit reagents at different times, or deposit them simultaneously and have them arrive at times dictated by their travel paths. Modifying channel lengths and widths is the easiest method, but is constrained by the device's footprint and available sample volume, as longer

and wider channels will require larger volumes. Alternatively, one can attempt to modify the speed at which liquid wicks through the paper itself. This is predominantly dictated by the pore size of the paper and is typically modified by adding material to block the pores, slowing flow. Further, one can have the liquid flow outside the paper altogether in some kind of external capillary. This work, on the other hand, investigated the use of a CO_2 laser to uniformly etch the surface of the paper. Depending on the degree of etching, this was able to both increase and decrease the wicking speed of water through paper channels.

The simplest lateral flow devices are typically colorimetric, giving qualitative results. However, getting quantitative data can be quite a bit more difficult. Distance-based devices provide a user-friendly means of obtaining quantitative data without the need for any additional equipment, simply by using an included ruler or calibrated markings. This work details the development of a quantitative DNA detection device that utilizes the aggregation of polystyrene microspheres to affect the distance that microspheres wick through filter paper. The microspheres are conjugated to ssDNA oligomers that are partially complementary to a target strand, and in the presence of the target strand, form a 3-strand complex, resulting in the formation of aggregates. The higher the concentration of the target strand, the larger the aggregate, and the shorter the distance wicked by the microspheres. This behavior was investigated across a wide range of target concentrations and under different incubation times to understand aggregate formation. The device was then used to successfully detect a target strand spiked in extracted plant DNA.

Table of Contents

LIST OF FIGURES

LIST OF TABLES

Chapter 1: Introduction

INTRODUCTION

Paper-based microfluidics is a field that promised complex microfluidic devices that are inexpensive, simple to use and manufacture and perform comparably to traditional glass and plastic microfluidic devices. Much research has been done in the past decade to advance the field towards that goal.

The focus of the research detailed in this dissertation is focused on utilizing the inherent properties of paper to further the development of paper-based microfluidic devices. A brief overview of paper-based microfluidics is found in Chapter 2. The first project, detailed in Chapter 3, explores modifying the surface of chromatography paper with a CO_2 laser to either enhance or impede the speed at which fluid wicks through the paper. This method of modifying the paper provides another tool for researchers to use in the development of complex fluidic circuits, such as those that require the automated, sequential delivery of different reagents to regions within the device. The second project, detailed in Chapter 4, involves the aggregation of polystyrene microspheres in the presence of a target nucleotide strand and the subsequent change in the distance the microspheres are able to wick through the paper, due to their aggregation. This change in distance wicked can be used to determine the concentration of the targeted strand.

Chapter 2: Paper-Based Microfluidics

INTRODUCTION

Over the past twelve years, the field of paper-based microfluidics has attracted considerable interest for its promises of providing low-cost, point-of-care diagnostic devices.[1-4] These paper-based devices offer similar functionality to traditional glass- and plastic-based microfluidic devices at a fraction of the cost. Such devices meet many of the WHO's ASSURED[5] (Affordable, Sensitive, Specific, User-friendly, Robust and rapid, Equipment-free, and Delivered) criteria, developed to detail the specifications for a diagnostic device to use in developing countries.

PAPER

Paper is a widely abundant resource with many properties that make it ideal for use as a microfluidic substrate. In particular, paper is a self-wicking material due to its porous capillary-like structure. This results in fluid driving its self through the device, without the need for external pumps such as those used in traditional plastic and glass microfluidics. This results in much easier to use devices. Paper is also very inexpensive, which encourages frequent and rapid iteration during the prototyping and design process. Finally, the patterning process of the paper itself can be very simple, from using crayons to define channels or using standard commercial office printers. These attributes all make paper the ideal substrate to use in resource-limited settings, such as those found in developing countries or space.

PATTERNING METHODS

There are a number of different methods used to define channels through which fluid will flow; however, most of these methods involve making hydrophilic channels with hydrophobic walls. These methods do limit the devices to use with aqueous solutions only, however, as nonpolar solvents will not be confined to the defined channels.

Paper-patterning techniques can be broadly classified into three major categories based on how they create hydrophilic channels and hydrophobic barriers. Paper, which is naturally hydrophilic, can be selectively made hydrophobic to define the boundaries of channels, usually done by impregnating the paper with a hydrophobic substance such as wax or a paper-sizing agent via embossing[6,7] or printing,[8-15] or photoresist when using lithographic techniques.[16,17] Channels can also be formed by selectively hydrophilicizing regions of paper that has been made completely hydrophobic. This has been done with inkjet printers[18,19] and laser treatement.[20] Plasma treatments have been developed for both techniques.[8,21,22] Finally, the third class of patterning techniques do not involve adding or removing any extra substances to the paper, it simply involves physically removing the unwanted regions of the paper. This can be done with a craft cutter[23,24] or a CO_2 laser.[25-28] Using a laser to cut the paper results in identical devices every time, as it doesn't deal with a physical blade that can dull. Removing material does make the devices more fragile than other patterning techniques.

DIAGNOSTIC TECHNIQUES

One of the most common types of paper-based devices are lateral flow devices, which generally only provide qualitative or semi-quantitative results.[3,29-33] Many existing quantitative devices require cameras to determine color intensity,[34,35] or multimeters to determine current[36] or resistance[37] changes, from which analyte concentrations can be determined. Distance-based methods, however, have been proposed to be the ideal solution for providing instrument-free, quantitative results.[32,38-45] These methods often utilize a color-changing reaction that occurs as fluid wicks along a channel, where the length of the colored region corresponds to the concentration of the targeted analyte.[32,40,46-51] The specific reaction used depends on the target analyte, requiring each new device to be designed for a different suitable reaction. Other distance-based methods utilize other mechanisms, such as fluid viscosity[52] or blood coagulation[53] affecting wicking speeds.

FLOW CONTROL

In order to develop devices capable of handling complex, multi-step (automated) detection chemistries, a variety of different fluid control techniques have been proposed and implemented.[54-57] In particular, the issue of sequential delivery is important. To achieve sequential delivery, one can manually deposit reagents at different times, or deposit them simultaneously and have them arrive at times dictated by the dimensions of their travel paths.

Fluid flow in paper is frequently described by the Lucas-Washburn equation,[58,59] which models paper as a bundle of capillary tubes, and describes the position of the liquid front as a function of the square root of time:

$$L(t) = \sqrt{\frac{\gamma D_c \cos(\theta)\, t}{4\mu}}$$

where γ is surface tension, D_c is the effective pore diameter, θ is the contact angle between the liquid and the paper (taken to be zero in a fully wetting material such as paper), and μ is the dynamic viscosity. While not physically accurate as to the actual microstructure of paper, the Lucas-Washburn model works reasonably well at predicting the flow.[60] Where the model fails is with channels with different or non-constant widths. In general, wider channels wick more quickly than narrower channels, but those with increasing widths result in a slowing of the wicking front[26,61] and conversely, those with decreasing widths have a faster wicking front velocity.[62,63]

For sequential delivery, modifying channel lengths and widths is the easiest method,[26,64,65] but is constrained by the device's footprint and available sample volume, as longer and wider channels will require larger volumes. The use of external shunts for wicking can also provide delays by effectively increasing the wicking length of the channel.[66]

However, in a channel of constant width, according to the Lucas-Washburn model, in order to either increase or decrease the wicking speed of a given liquid, the only parameter that can be changed is the effective pore diameter. Because of this, most research into flow control has been focused on introducing delays, through techniques such as the addition of soluble[67,68] or insoluble[14,69,70] barriers, or compression[71] (resulting in smaller pores). However, delaying the flow can be problematic due to increased evaporation leading to sample loss, which requires an increased sample volume to counter.

The other option, speeding flow, is challenging, as it is difficult to increase the pore diameter. Typically, the maximum wicking speed is tied to the material choice. To increase wicking speeds beyond the limits of a given substrate, most attempts have focused on having the fluid travel outside the paper in external capillaries, either by sandwiching the paper between polymer films,[72,73] creating a two-ply structure,[74] or by removing portions of the paper to create empty channels for the liquid to flow through.[75-78] These techniques can result in much faster wicking, as much of the liquid is able to bypass the paper matrix entirely. This is ideal for devices that require rapid transport of large volumes of liquid between different regions of the device, but such behavior may be problematic or unsuitable for devices that utilize immobilized detection reagents or use small liquid volumes.

Chapter 3: Laser-Etching

INTRODUCTION

The simplest paper-based devices are lateral flow devices, where liquid wicks in one direction along the paper strip. These are suitable for simple detection chemistries; however, for more complex reactions, devices that are more complicated are required, and this frequently entails the sequential delivery of different liquids or reagents to reaction zones.

In this chapter, a CO_2 laser is used to uniformly etch the surface of the paper, increasing its effective pore diameter and thus its wicking speed. By adjusting the grayscale levels of the design etched onto the paper, the resulting wicking speeds can be increased or decreased.

Methods and Materials

The layout of the channel array was designed using graphical software (CorelDraw, Corel Corportation, Ottawa, ON, CA) and cut out and etched using a 30W CO_2 laser (Zing 16, Epilog Lasers, Golden, CO) onto Whatman #1 Chromatography (GE Healthcare, Chicago, IL) paper. The laser raster settings were 13% power, 45% speed, 500 dpi, and Floyd-Steinberg dithering and the vector settings were 7% power, 60% speed, and 5000 Hz. These settings correspond to the highest values that reliably did not completely burn through the paper at 100% grayscale values. Grooves were made with 5% power, 100% speed, and 5000 Hz. Etching levels were controlled by the grayscale value of the channel fill, ranging from 0% (pure white) to 100% (pure black). The channels were 3 mm wide and 40 mm long. Mass loss was measured by weighing 50 mm x 50 mm squares etched at each grayscale value and comparing them to identically sized unetched squares. Wicking

experiments were performed in a humidity-controlled chamber kept at 55% RH and 23°C. [60] DI H_2O was wicked and the fluid front recorded. See Figure 3-1 for the experimental wicking setup.

Figure 3-1. Wicking experimental setup. A) Wicking was performed in a humidity-controlled chamber kept at 55% RH and 23°C. DI H_2O was wicked vertically in each channel to eliminate any potential effects caused by a backing. B) Close-up view of the test device, with seven 3 mm wide, 40 mm long channels, etched at 0% (unetched), 75%, 80%, 85%, 90%, 95%, 100% grayscale values. Scale bar is 5 mm.

Demonstration Device

The demonstration device was first printed using a solid wax ink printer (Colorqube 8880DN, Xerox Corporation, Norwalk, CT) and then placed in an oven at 170°C for 2 min to melt the wax, forming hydrophobic barriers. After melting, the devices were cut and etched with the laser cutter. Devices were then backed with packing tape and rounds of Whatman #17 chromatography paper were used as sample pads. The fabrication process flow of the devices is depicted in Figure 3-2. The wicking fluids were 100 µL of each of the following dyes: 5 mM Erioglaucine-disodium salt, 5 mM tartrazine, and 5 mM Allura Red [79,80]. Channels were 3 mm wide with the two outer legs of equal length (~50 mm), and a shorter center channel (~40 mm).

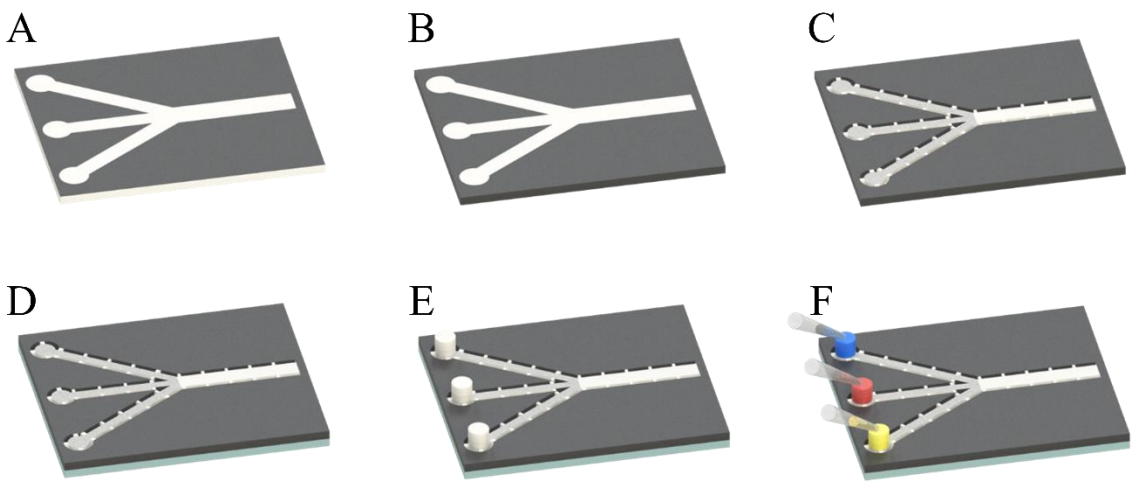

Figure 3-2. Fabrication process flow for demonstration device. A) Devices were printed using a solid wax printer onto Whatman #1 Chromatography paper. B) The wax was melted by placing the paper into an oven at 170°C for 2 minutes. C) The paper was etched and the channels were cut to final dimensions. The presence of the side-struts along the edge of the channels are for support, preventing the wet channels from buckling and lifting up from their backing. D) The bottom side of the devices were coated with packing tape to form a backing. D) Rounds of Whatman #17 Chromatography paper were used as sample pads to regulate flow into the channels. F) 100 µL of 5 mM dye were introduced into each channel simultaneously using a multi-channel pipette.

Results and Discussion

The laser etching works by converting a grayscale image to a black and white image through dithering, where the average density of individual black dots will match the original grayscale value. The laser then rasters the image onto the paper, removing material from the surface of the paper. This is shown in Figure 3-3.

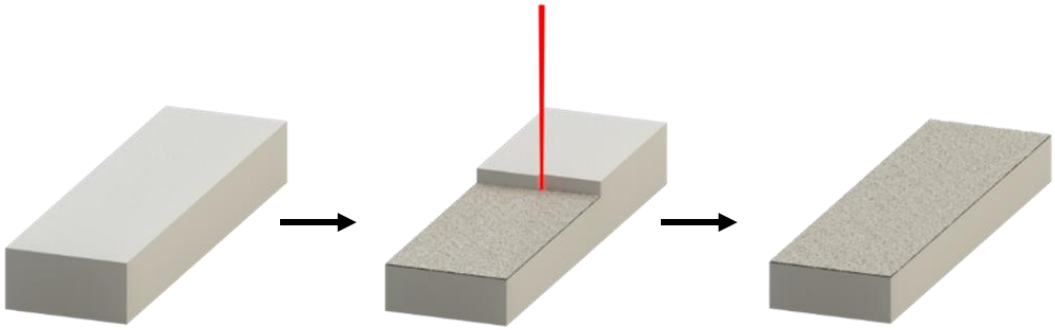

Figure 3-3. Schematic of the etching process. The etching process removes material evenly from the top surface the paper.

The effect of the etching process on the chromatography paper is shown in Figure 3-4. While there are few visible differences at the macro scale between 0% (unetched) and 50% etched, the SEM image shows that at 50%, much of the material in between surface fibers has been removed. Surface remodeling becomes more significant as grayscale values increase, and at 100%, the paper is visibly perforated at the macroscale.

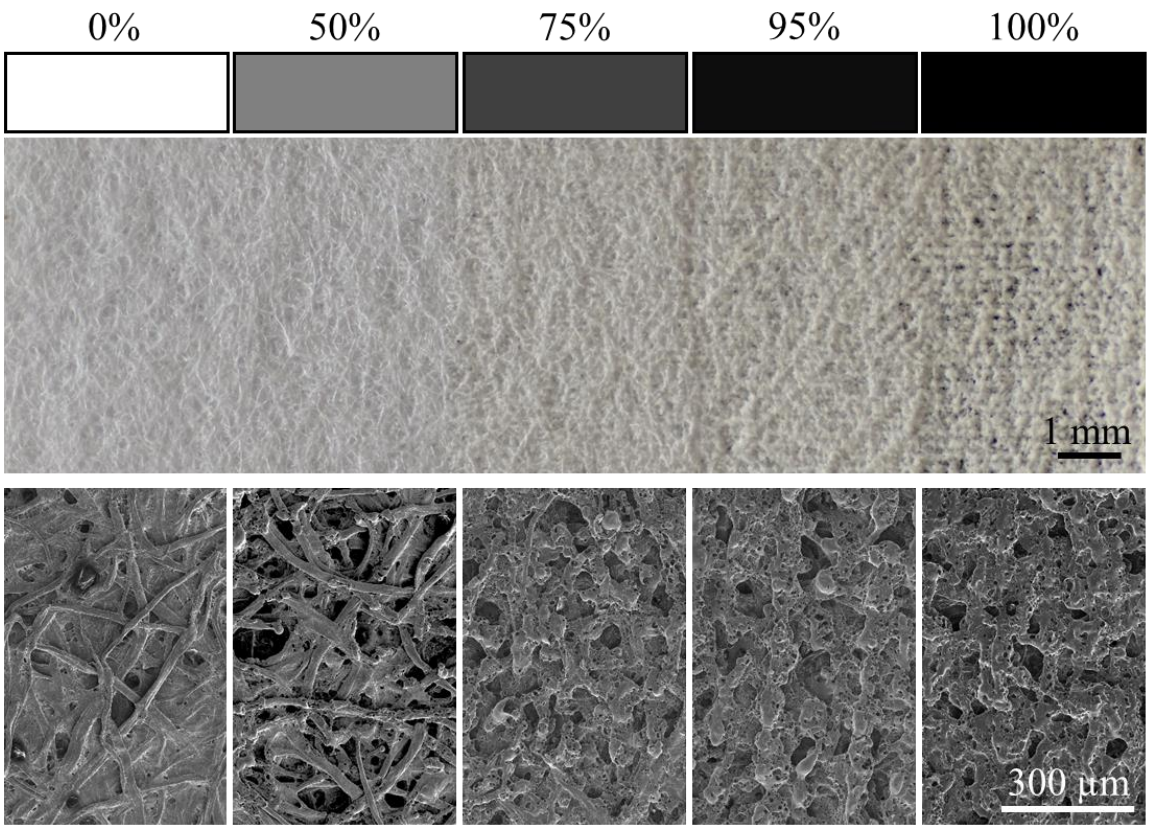

Figure 3-4. Macro and SEM images of the etched paper surface. At the macro level, surface modification is not visible until etched at a grayscale value of 75%, but even at 50%, it is apparent that material has been removed from the surface in the SEM images. By 100%, holes are being burned through the thickness of the paper.

A closer look at the extensive surface remodeling occurring at higher etching levels is shown in Figure 3-5. In it, the etched region contains highly fragmented remains of fibers that are coated with a smooth material. This material is likely soot, as it disappears, revealing the highly porous fibers underneath, when washed in water (Fig. 3-6)

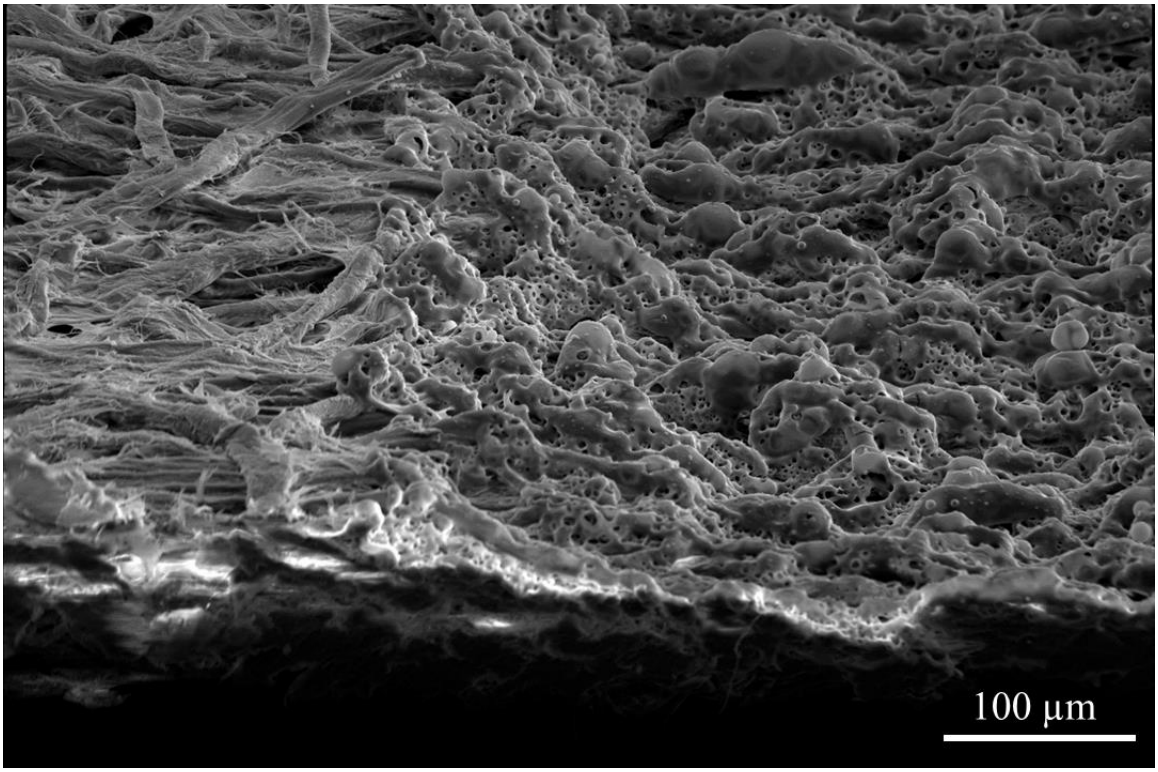

Figure 3-5. Unwashed Etched Chromatography Paper. The left side is unetched paper, while the right has been etched at 100%. The smooth material on the fibers on the right is soot.

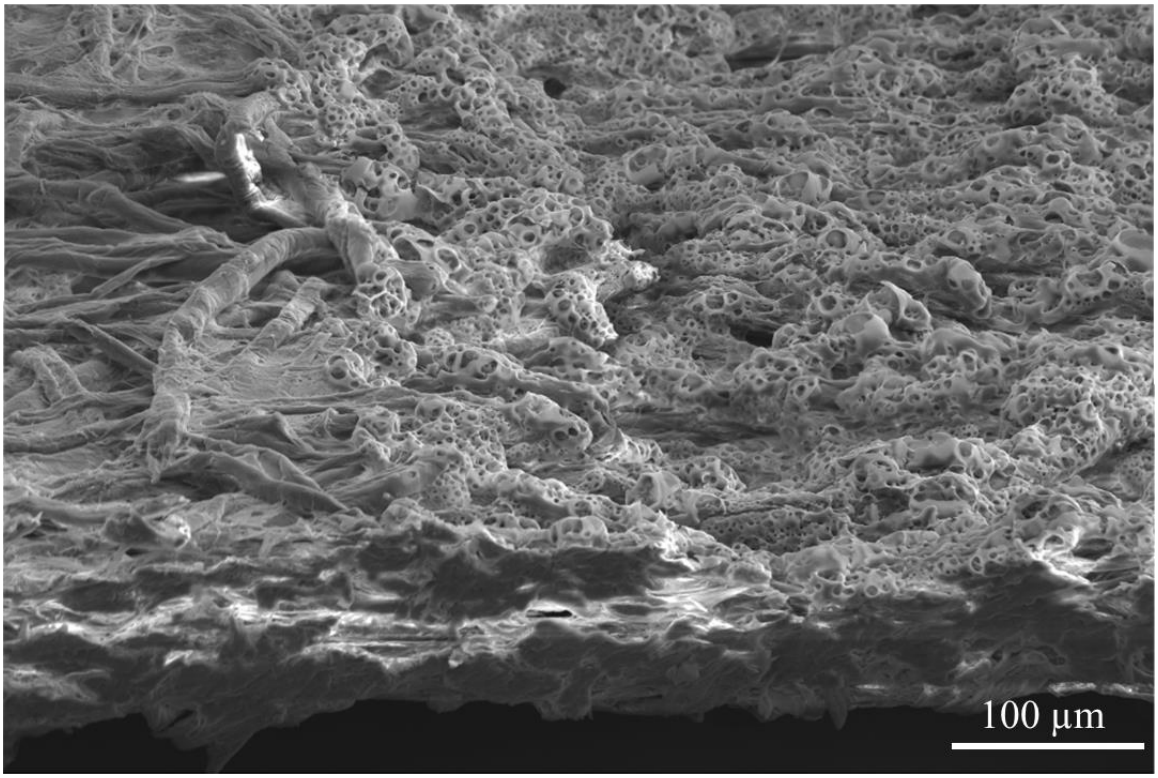

Figure 3-6. Washed Etched Chromatography Paper. The left side is unetched and the right side is etched at 100%. The entire paper was rinsed in DI H_2O before being left to air dry. The highly porous hollow structure of the remaining surface fibers on the right are exposed after the soot has been washed away.

While the SEM images show a noticeable difference in surface topology between the 0% and 50%, the actual mass loss at 50% is negligible, as seen in Figure 3-7A. The mass loss increases from approximately 4% at 75% grayscale to approximately 40% at 100% grayscale. Due to this, the grayscale values used for the wicking experiments were limited to values above 75%. In general, the fastest wicking occurred in the 75% channels and wicking speeds decreased as the level of etching increased, ultimately resulting the 100% channel wicking even slower than the unetched channel. This can be seen in Figure 3-7B.

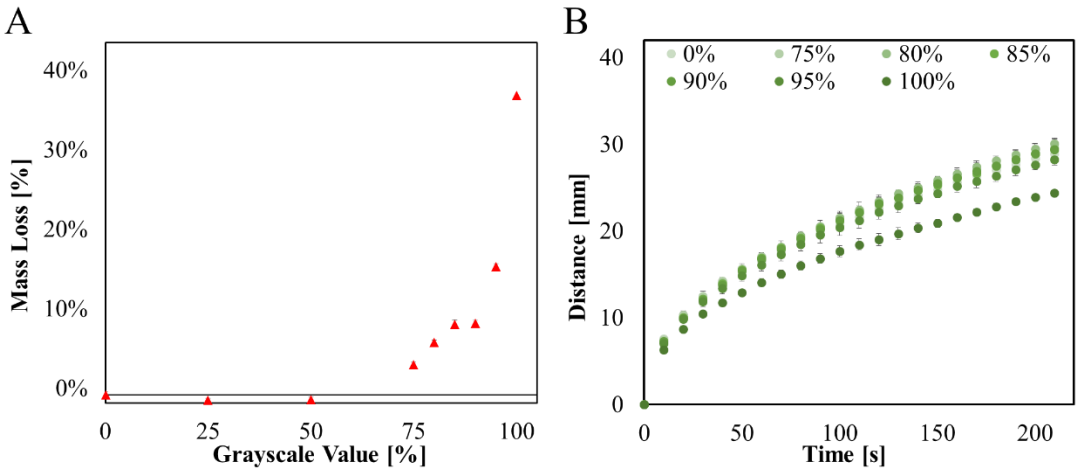

Figure 3-7. Single-Sided Etching. A) Percent mass loss at each etching level of single-sided etched paper. 50 x 50 mm squares of Whatman #1 Chromatography paper were weighed after being etched at each grayscale value. Data presented as mean ± SD. N=10 B) Average wicking distance vs time at each etching level of single-sided etched paper. Each channel is 3 mm wide. Wicking was performed at 55% relative humidity and constant 23°C. Data presented as mean ± SD. N=3.

The above data suggests that there are two competing phenomena being observed. The first is an increase in wicking speeds due to a more porous surface and a decrease in wicking speeds due to increased mass losses at higher etching levels, resulting in reduced cross-sectional areas. The degree of thickness reduction can be seen in Figure 3-8.

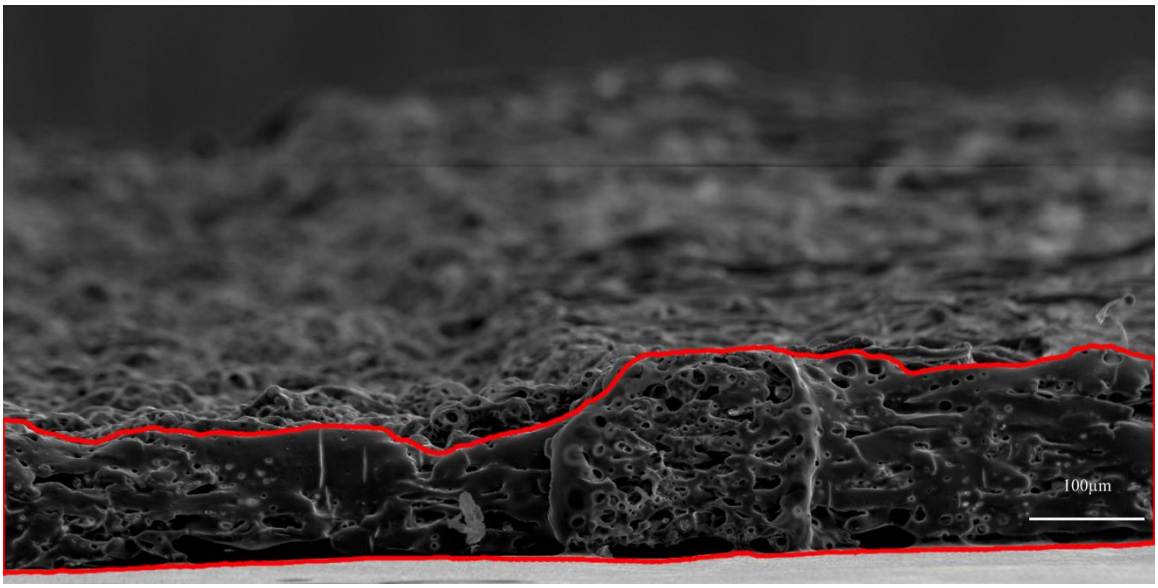

Figure 3-8. Reduction of Paper Thickness. SEM image showing the effect of etching on the cross-sectional area of the paper. The region on the left has been etched at 100% while the region on the right has not been etched.

To further enhance the benefit of the more porous surface, wicking was investigated in paper etched on both sides. As shown in Figure 3-9A, the mass loss trend is quite similar as the single-sided etch paper, with very small mass losses below 75%. Paper etched on both sides at 100% disintegrated, so no value was able to be obtained. A direct comparison between the two can be seen in Figure 3-10. As with the single-sided etched paper, the fastest double-sided channel was the 75% channel and speeds decreased as etching increased, up to 95%, which was much slower than the unetched channel. This can be seen in Figure 3-9B.

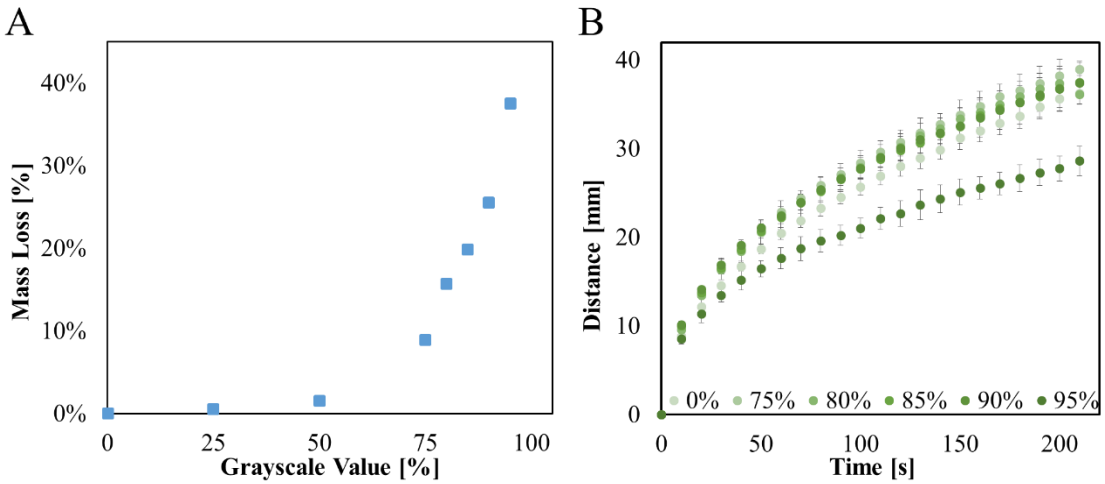

Figure 3-9. A) Percent mass loss at each etching level of double-sided etched paper. 50 x 50 mm squares of Whatman #1 Chromatography paper were weighed after being etched at each grayscale value. Data presented as mean ± SD. N=10. B) Average wicking distance vs time at each etching level of double-sided etched paper. Each channel is 3 mm wide. Wicking was performed at 55% relative humidity and constant 23°C. Data presented as mean ± SD. N=3.

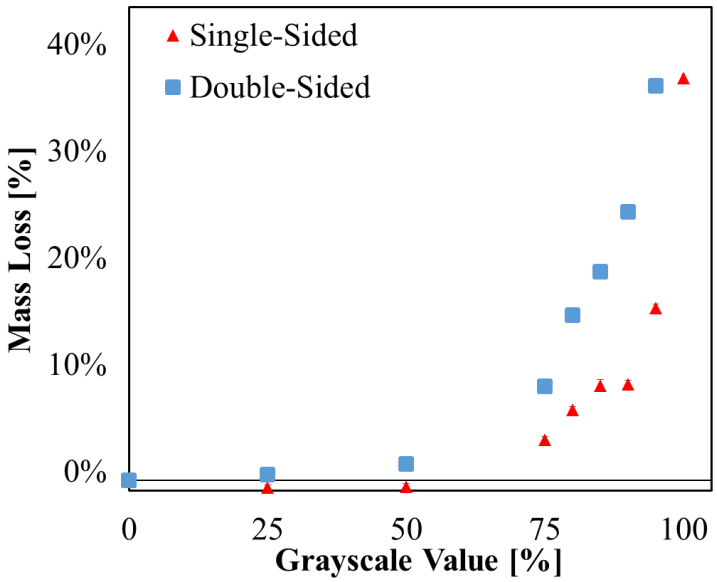

Figure 3-10. Percent mass loss at each etching level of single- and double-sided etched paper. 30 x 30 mm squares of Whatman #1 Chromatography paper were weighed after being etched at each grayscale value. At each grayscale value, the mass loss experienced by the double-sided etched paper is approximately twice that of the single-sided etched paper. No data exists for double-sided 100% as the paper disintegrated at those etching levels. Data presented as mean ± SD. N=10.

Comparing the single- and double-sided channels directly, as in Figure 3-11, shows that at 75%, the double-sided channel is much faster than the single-sided channel (Fig. 3-11A), but as the etching level increases, that difference gets smaller and at 95% (Fig. 3-11B), the two channels behave quite similarly, despite the double-sided channel having twice the mass lost as the single-sided. However, when comparing two conditions under which the paper had lost approximately the same amount of mass (~38%), the single-sided 100% and double-sided 95% did not behave similarly; instead, the double-sided channel was considerably faster (Fig. 3-11C). These both suggest that the effects of the more highly porous surface are beneficial to faster wicking, but work in opposition to the effects of the reduced cross-sectional area, which impedes flow.

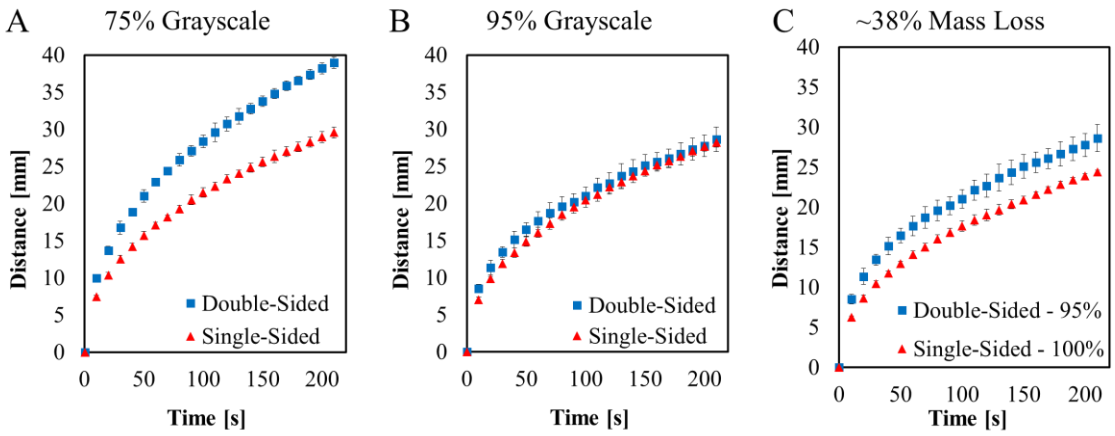

Figure 3-11. Average wicking distance vs time at select etching levels of both single- and double-sided etched paper.

XPS spectra analysis was performed to verify that the laser etching process had not altered the chemical composition of the surface. Laser-etched paper had an approximately 30% reduction in intensity of the carbon-carbon peak at 284.8eV compared to the unetched paper and had a peak appear at approximately 283eV that

is suspected to correspond to soot, as it disappeared from samples that were rinsed in water after etching. The full carbon spectra can be found in Figure 3-12.

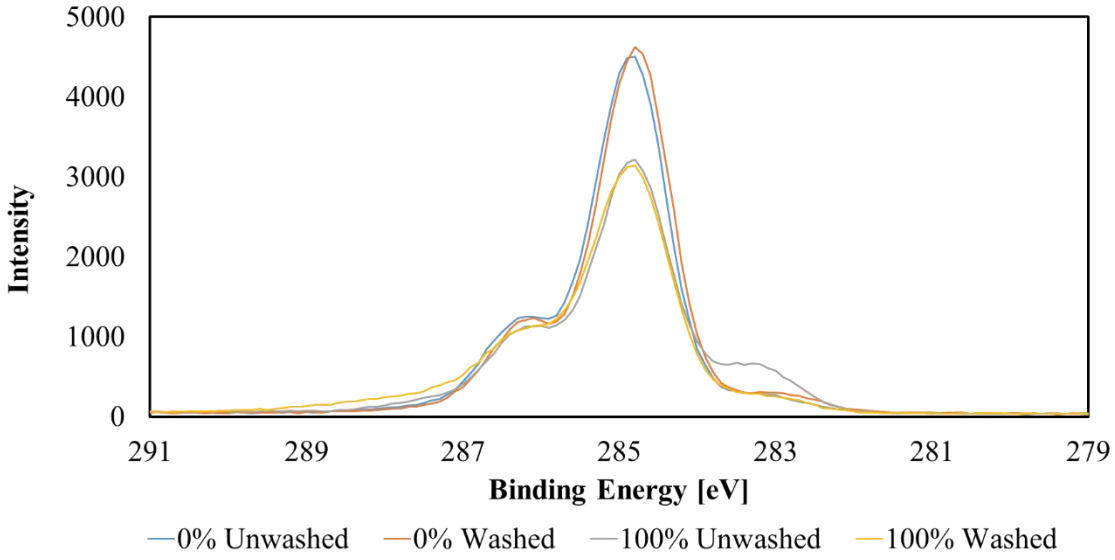

Figure 3-12. XPS Carbon 1s spectra of laser-etched Whatman #1 Chromatography Paper. The washed paper was simply dipped into DI H_2O and allowed to dry at room temperature.

All of the data presented above are from vertical wicking, while the majority of paper-based microfluidic devices are used horizontally. In order to confirm that the vertical results were applicable to horizontal devices, a simple three-channel device was designed that demonstrates the technique's utility in enabling sequential delivery.

Unmodified, the central channel should reach the intersection first, followed by the simultaneous arrival of the other channels. However, by etching different channels at different levels, not only can the relative arrival times of each channel be modified, but also their absolute wicking times. Figure 3-13 shows a time-lapse comparison of a device with unetched channels (0-0-0) and one with the two outer legs etched at 75% with the center leg remaining unetched (75-0-75).

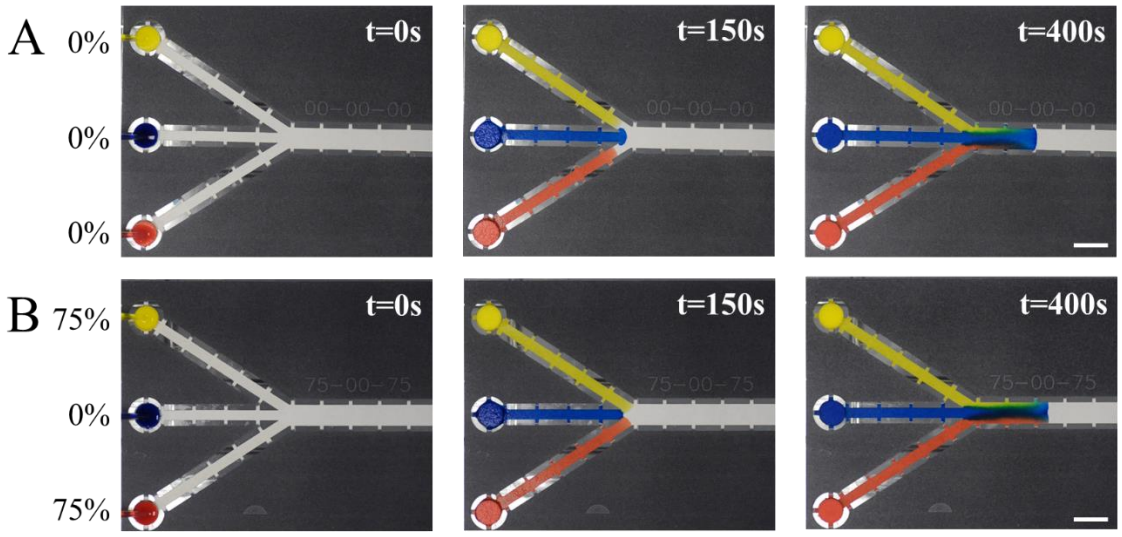

Figure 3-13. Time-lapse of the single-sided etched three-channel demonstration device. A) All channels are unetched. The middle channel arrives at the intersection first, followed by the top and bottom channel that arrive nearly simultaneously. B) The outer channels are etched at 75% and the middle channel is unetched. The outer channels arrive at the intersection simultaneously, while the middle channel takes a bit longer. Scale bars are 1 cm.

In the 0-0-0 device, all channels wicked the dyed solutions at the same speed; however, since the center channel was shorter, the blue solution reached the intersection first, followed by the simultaneous arrival of the red and yellow solutions. In the 75-0-75 device, the dye in the etched channels wicked much more quickly than in the unetched channel. The yellow and red dye reached the intersection simultaneously, and arrived much sooner than the blue dye in the center unetched channel. Comparing the two different devices at T=400s, one can see the consequence of the different fluid arrival times in regards to the degree of mixing of the different dyes. In the 0-0-0 device, after the intersection, the blue dye dominates and the other dyes slowly enter from the sides, whereas in the 75-0-75 device, the blue dye is washing the red and blue dye further along the channel.

The wicking speeds in the demonstration device were, however, much faster than their corresponding vertical wicking speeds. The most likely cause for this discrepancy is the excess of liquid that races across the surface of the paper upon deposition. As noted before, traveling outside the paper is much faster than wicking through the paper. However, it is possible that vertical wicking is somehow hindered by gravity. To attempt to identify the role that the angle of the paper played on overall wicking speeds, vertical wicking tests were repeated with additional samples at 30°, 60°, and 90° from the vertical. Additionally, channels with varying numbers of lengthwise grooves were tested, as the grooves would provide a more streamlined path for excess liquid to travel through at shallower angles. The tests were also performed with the channels sealed in packing tape.

Figure 3-14 shows the time it took liquid to wick the full 4 cm length of the channels at the various angles for both single- and double-sided etched paper. For the channels without tape sealing, there was no consistent trend with respect to angle. Each angle resulted in substantial inconsistencies. However, once sealed with tape, the wicking times for the 0°, 30°, and 60° channels were remarkably consistent. Further, they displayed a trend of increasing speed with increasing etching level, unlike the untaped channels which showed the fasted wicking with more moderately etching levels of 75-95%. The 90° channels were slower at lower etching levels, but this is likely due to the differences in how liquid was delivered to the horizontal channels. The horizontal channels could not be dipped in a liquid reservoir, so instead, a saturated polyester sponge was lowered onto the channels to deliver the liquid. The sponge method resulted in slow initial wicking as the sponge settled onto

the paper, a slower process than the formation of the meniscus across the edge of the paper when dipping it into a reservoir.

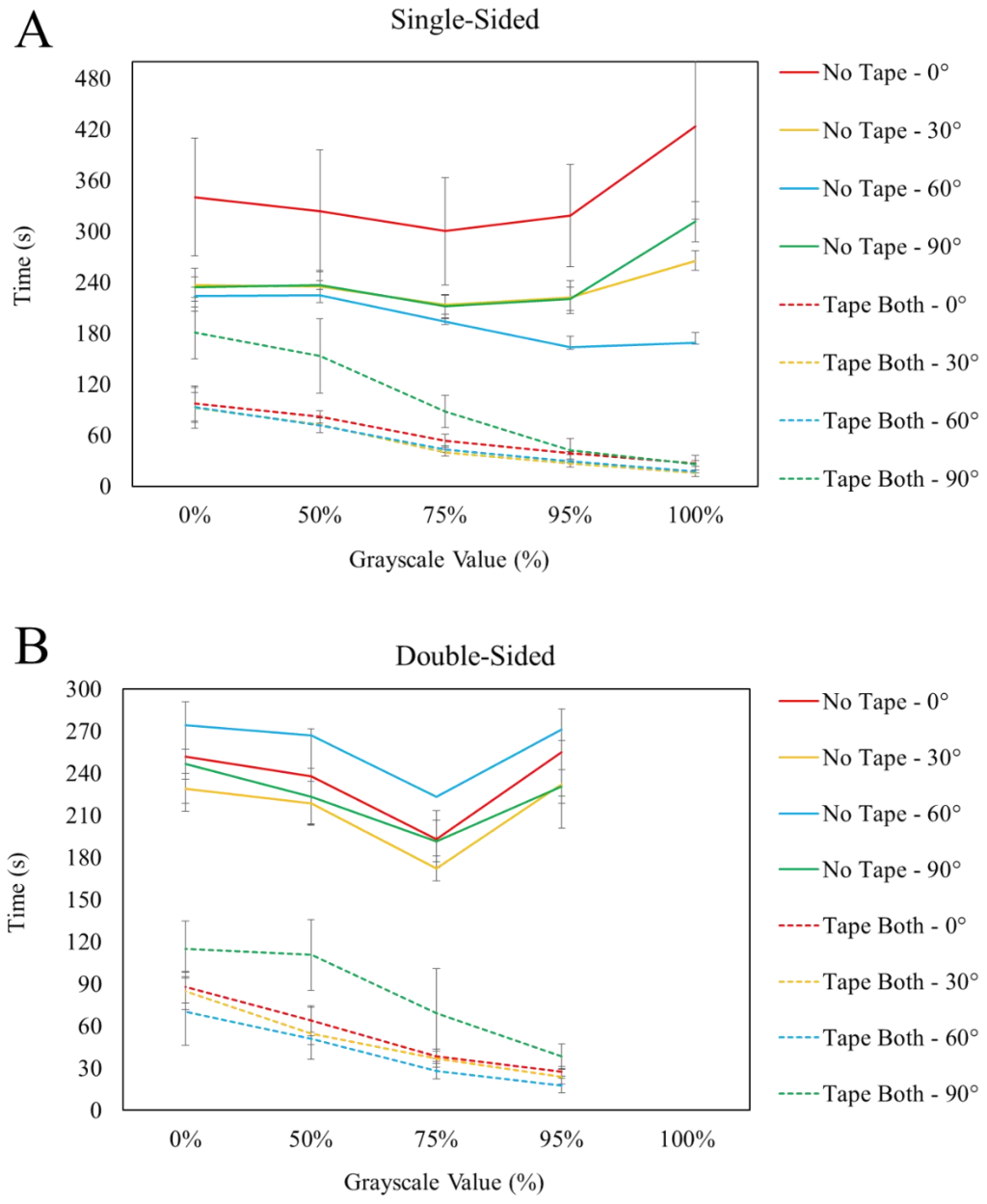

Figure 3-14. Wicking performance of single- and double-sided etched channels. N=5.

Figure 3-15 shows the time it took liquid to wick the full 4cm length of the channels at the various angles for channels containing 0, 1, 3, or 7 lengthwise grooves etched into the

surface of the paper. Unlike the raster etched channels, these channels show a clear trend of faster wicking with more grooves, both with and without the tape sealing.

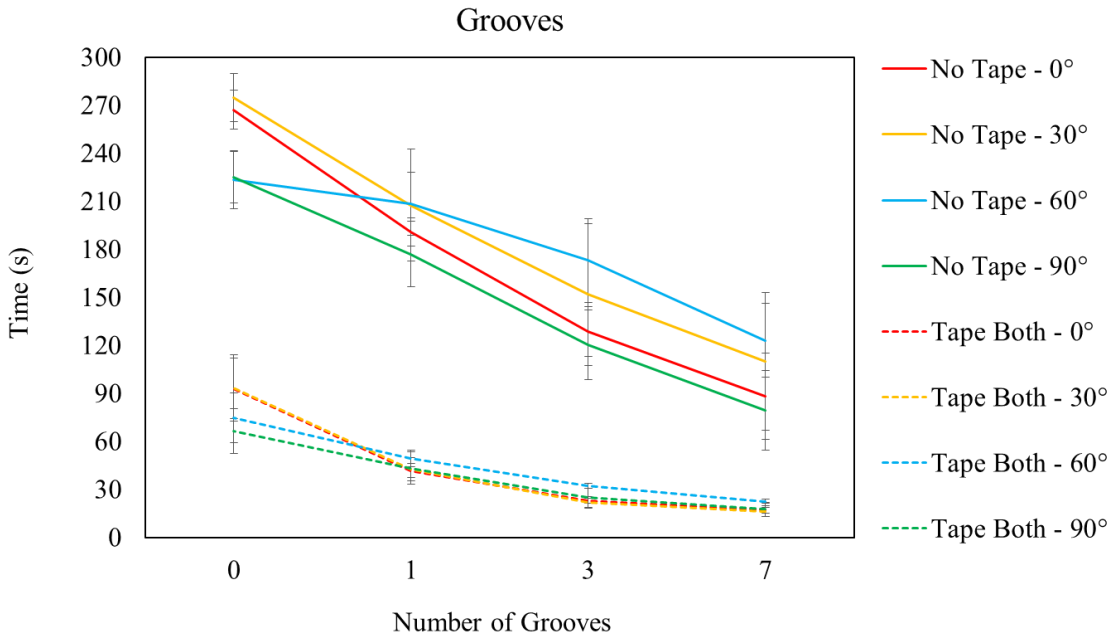

Figure 3-15. Wicking performance of channels with lengthwise grooves. N=5.

The above work details the use of laser etching as a means to control the wicking speed of liquid in paper-based microfluidic devices, where it can increase wicking speeds by as much as 10% and slow them by as much as 20%. The exact mechanisms behind the observed behaviors are not yet well understood and requires further investigation. The etching process can be performed in conjunction with the patterning of device channels themselves, resulting in a simplified fabrication process. As a proof of concept, we demonstrated the technique's utility in enabling sequential fluid delivery in a simple, three-legged device. In more complex devices, in addition to different etching levels in each channel, portions of individual channels can be etched to different degrees, resulting in highly tuned fluid delivery for specific applications, all without changing the overall device

footprint or channel geometry. Additionally, it is likely that by combining etching with geometric patterning, such as cutting through holes in the middle of channels, a much greater range of wicking control will be available through a single fabrication step.

Chapter 4: Distance-based DNA Detection

INTRODUCTION

Here we build upon our previous work[81] and investigate the process of aggregate formation and the viability of detecting targeted DNA in extracted plant material. The mechanism behind this detection method is the target-induced aggregation of two populations of microspheres; each conjugated to non-complementary DNA oligomer probes (Fig. 4-1). The probes are each partially complementary to the target analyte. Upon addition of the target to a mixture of the microspheres, they begin to aggregate. Unaggregated, the microspheres are small enough to wick through the paper substrate unimpeded, but when aggregated, there are both fewer available microspheres to wick through the paper and the aggregates themselves are too large to wick through the paper's pores. The degree of aggregation directly affects the distance wicked; with larger aggregates (caused by higher analyte concentrations) resulting in shorter wicked distances.

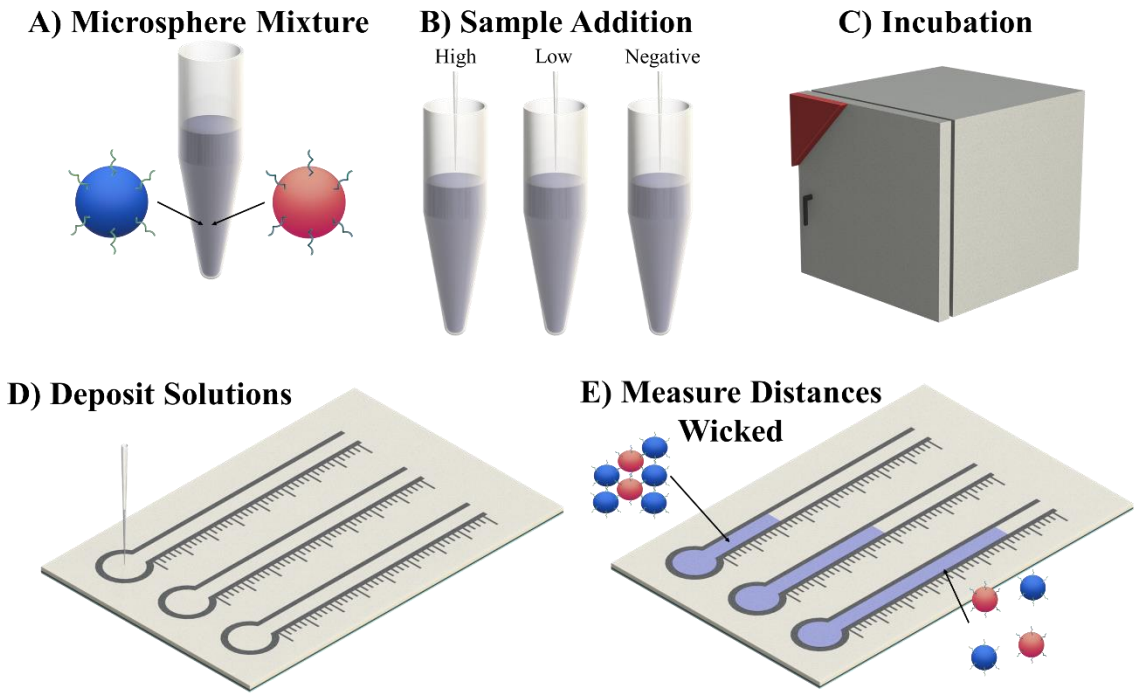

Figure 4-1. Process flow of the proposed microsphere aggregation and distance-based single-stranded DNA detection scheme. A) Microspheres conjugated to two different non-complementary oligomers are mixed together. B) Samples containing the targeted strand are added to the microsphere mixture. C) The microsphere solution is incubated at 45°C for 30 min. D) The microsphere solution is deposited in the channel inlet, where channels have been defined using solid wax printing. E) The microspheres in solutions containing the target strand have aggregated, resulting in reduced wicking distances.

Materials and Methods

Paper-based Microfluidic Device Fabrication

The devices were patterned in SolidWorks (Dassault Systèmes, Vélizy-Villacoublay, France) and printed onto Whatman grade 4 filter paper (GE Life Sciences, Pittsburgh, Pennsylvania USA) using a solid wax ink printer (ColorQube 8880; Xerox, Norwalk, Connecticut, USA). The wax was then melted in an oven (FD 53, Binder, Tuttlingen,

Germany) at 170ºC for 2 minutes, allowing it to penetrate the thickness of the paper. The paper was then run through the printer again, printing a solid layer of wax across the bottom side. The bottom of the paper was then sealed using packing tape to prevent leakages. The ruler markings have a 2 mm spacing. Figure 4-2 depicts the device's layered structure. The 40 mm x 3 mm channel and 7 mm diameter inlet require approximately 30 µL of liquid to reach the end of the channel.

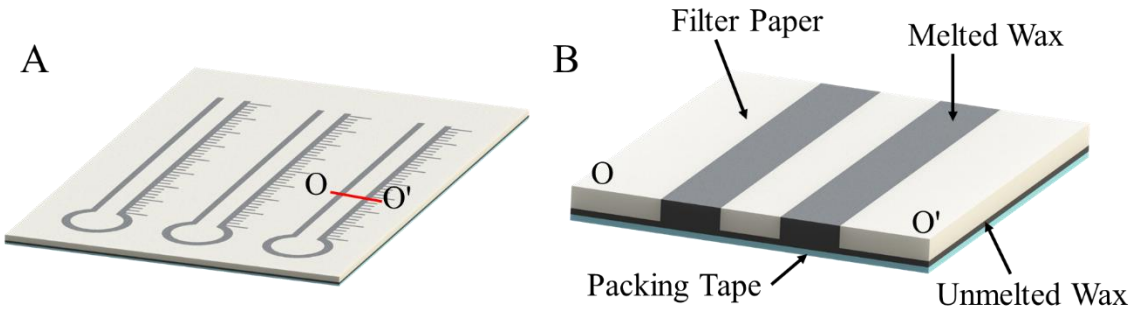

Figure 4-2. Structure of the assembled device. A) Fabricated device. B) Cross-sectional view.

Conjugation of ssDNA to Microspheres

Stock 10% solid 1 µm polystyrene latex carboxylated microspheres (Magsphere, Pasadena, California, USA) were washed 3x in 10 mM 2-(N-morpholino) ethanesulfonic acid (MES) and diluted to 3% solid. The microsphere solution was then mixed with one of the ssDNA probes (Probe A or Probe B) at a 1:4 probe to surface carboxyl ratio and excess 1-ethyl-3-(3-dimethylaminopropyl) carbodiimide (EDC) and N-Hydroxysuccinimide (NHS). After a 30 min incubation, additional EDC and NHS was added before another 30 min incubation period. Afterwards, the microsphere solution was washed once in 1% Tween-20 in 10 mM phosphate-buffered saline (PBS), returned to 3% solid, and then

washed 2x in 10 mM PBS. The sequences of all strands used in this study are listed in Table 4-1.[82] All chemicals were purchased from Sigma-Aldrich (St. Louis, Missouri, USA) and DNA was purchased from Integrated DNA Technologies (Coralville, Iowa, USA).

Table 4-1: Probe and target sequences

Name	**Sequence**
Probe A[82]	5'-/5AmMC6//iSp18/TTT TTT TTT TCG CAT TCA GGA T-3'
Probe B[82]	5'-TCT CAA CTC GTA TTT TTT TTT T/iSp18//3AmMC7/-3'
A'-B'[82]	5'-TAC GAG TTG AGA ATC CTG AAT GCG-3'
Strand C*	5'-CCG TGG TAG TGT ATC CTG AAT GCG-3'
Strand D*	5'-CCG TGG TAG TGT CAG TGT CGT GTT-3'

*Strands C and D were generated randomly for this study.

DNA Extraction from Plant Leaves

DNA was extracted from sour orange (*Citrus x Aurantium*) leaves using Plant DNAzol (Thermo Fisher Scientific, Waltham, Massachusetts, USA) using the manufacturer's recommended protocol (Fig. 4-3). Briefly, leaf tissue was homogenized using a mortar and pestle. Homogenized tissue was then mixed with DNAzol and chloroform before centrifuging at 12,000 g for 15 min. The upper aqueous phase was then removed and DNA was precipitated using 100% ethanol. The DNA was pelleted via centrifugation at 5,000 g for 4 min and then washed with a 1:0.75 DNAzol:ethanol solution, followed by a wash with 75% ethanol. The DNA was then dissolved using 8 mM NaOH (100 µL per 200 mg of leaf tissue) and neutralized using HEPES buffer. DNA concentration of the extracts

ranged from 90-130 ng/µL. Extracts were spiked with our target strand, A'-B', before or after the extraction process. All chemicals were purchased from Sigma-Aldrich (St. Louis, Missouri, USA).

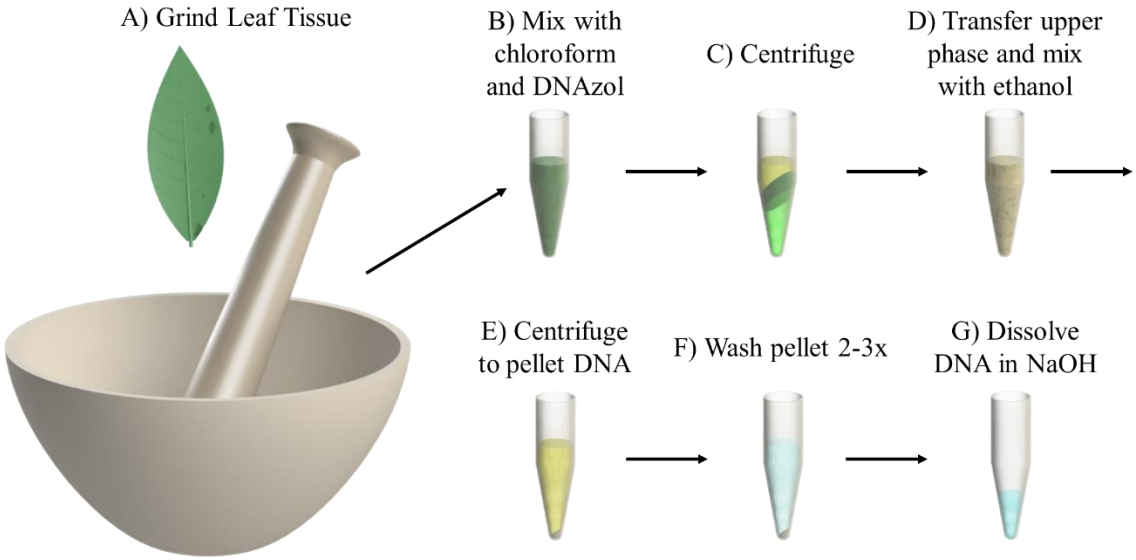

Figure 4-3. DNA extraction process flow using Plant DNAzol.

Wicking Test Protocol

Microsphere solutions (30 µL, 2% solid) comprising equal parts Probe A-conjugated microspheres, Probe B-conjugated microspheres, and target strand (A'-B'), were incubated for 30 min at 45°C to promote hybridization and then deposited in the inlets of 2 mm wide wax-printed paper-based microfluidic channels. The channels were left to wick for approximately 15 minutes in a humidity chamber (Model 5503; Electro-Tech Systems, Glenside, Pennsylvania, USA) kept at 55% RH and 23°C. For ease of differentiating which probe was conjugated to which set of microspheres, red and blue microspheres were used. For the fluorescent tests, red and green fluorescent microspheres were used instead.

Aggregate Size Analysis

Custom 1 µL wells were constructed using laser-cut 0.5-mil polyamide tape (Caplinq, Orléans, Ontario, Canada) stuck to glass microscope slides. Wells were capped with an ultrathin (0.085-0.115 mm) coverslip (Thorlabs, Newton, New Jersey, USA) and observed under 100x magnification using a DM2000 fluorescent microscope (Leica Microsystems, Wetzlar, Germany). The aggregate observation wells are depicted in Figure 4-4.

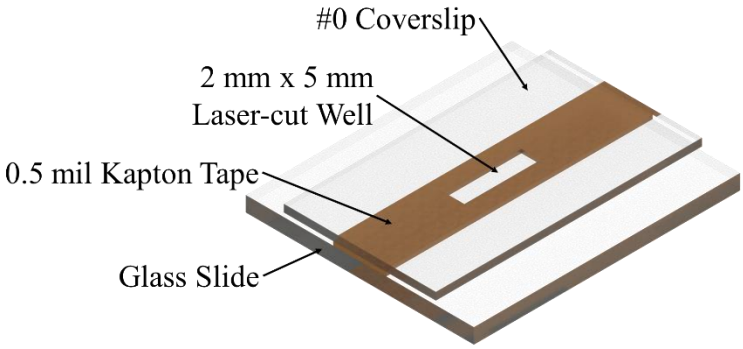

Figure 4-4. Microsphere aggregation observation well.

Results and Discussion

Size-based Wicking

The Whatman grade 4 filter paper chosen for these experiments is described as having a particle retention size of 22-25 µm. This is a descriptor of a filter paper's filtration and does not correspond to the sizes of particles capable of lateral wicking. Figure 4-5 depicts the relative difference in wicking distances of solutions containing 2% solid microspheres of different sizes. The smallest microspheres, 150 nm, traveled the furthest, over 40 mm, while the largest microspheres, 10 µm, were too large to wick at all and sat on the surface of the paper. The 1 µm microspheres were chosen for subsequent experiments, as

preliminary studies found that the 150 nm microspheres did not readily form aggregates large enough to significantly change their overall wicking distance.

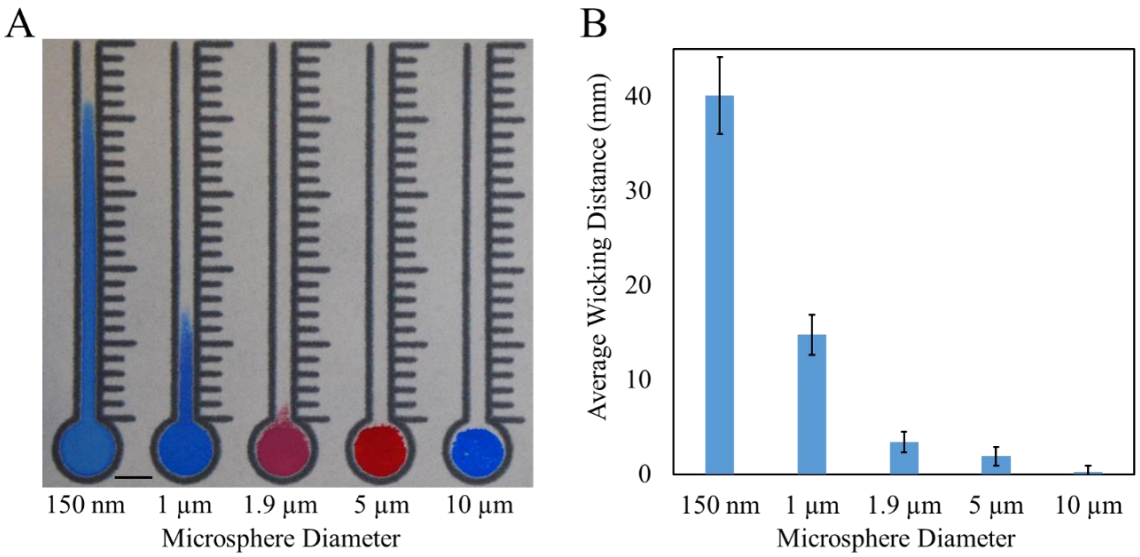

Figure 4-5. Size-based Wicking. A) Wicking distances of 2% solid microsphere solutions in the paper channels. 30 µL of microsphere solution was added to the center of each inlet. Scale bar is 5 mm. B) Average wicking distances measured from the top of the inlet. Data displayed is mean ± standard deviation. N=10.

Microsphere Concentration

In order to determine how wicking distances were affected by microsphere concentration, two experiments were run using the 1µm microspheres. The first maintained a constant volume (30 µL) with varying concentrations while the second kept the number of microspheres constant as the concentration (and overall solution volume) changed. Solutions containing 1%, 2% and 3% solid microspheres were tested. When volumes were held constant, decreasing microsphere concentration resulted in channels that were more pale and wicked slightly shorter distances (Fig. 4-6A); however, when microsphere quantities were held constant, as the concentration of microspheres decreased (and volume

increased) the distances wicked increased (Fig. 4-7A). As shown in Figures 4-6B and 4-7B, the actual volume of liquid used seems to play a larger role in wicking distances rather than the actual quantity of microspheres. Larger volumes (and corresponding lower microsphere concentrations) were tested, but almost universally leaked, as their volumes exceeded the channels' capacity. This excess liquid eventually leaked through the unmelted wax barrier at the bottom of the channel and slipped under the melted wax walls.

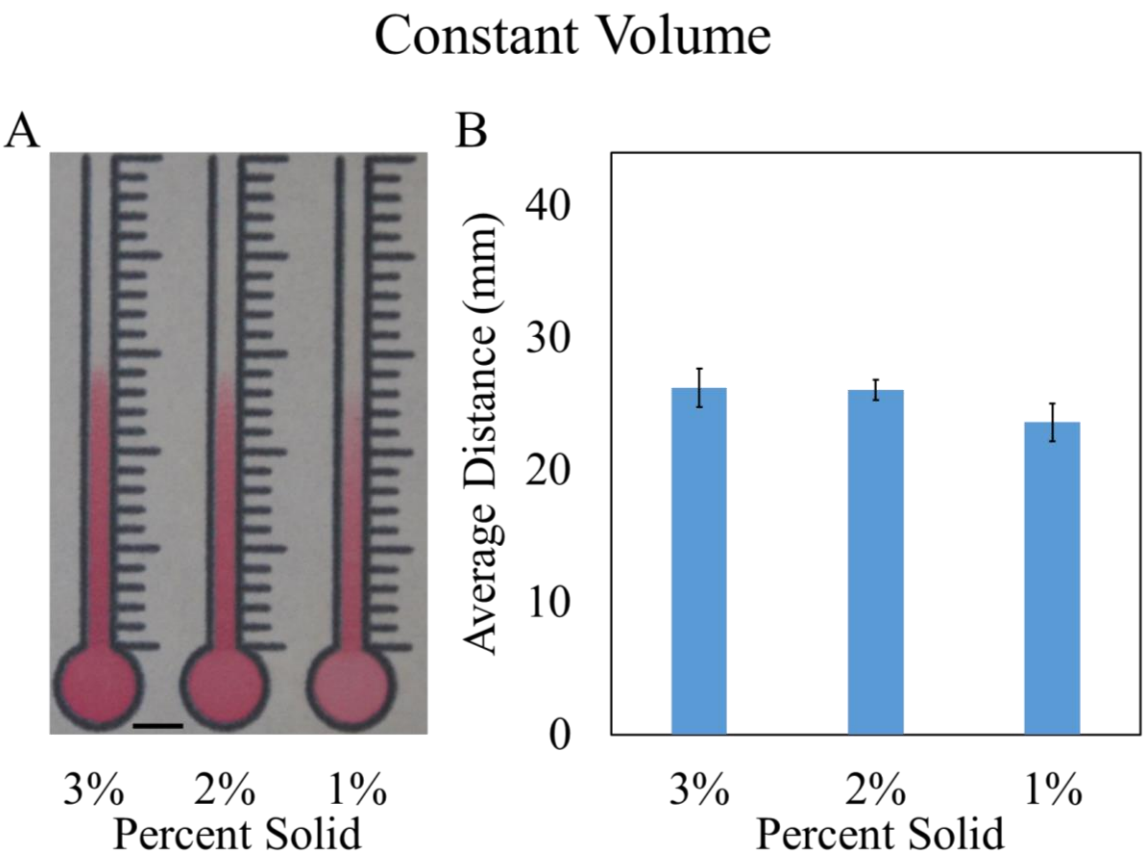

Figure 4-6. Microsphere Solution Optimizations - Constant Volume. A) Wicking distances of 1-3% solid microspheres in the paper channels when the volume liquid deposited in each channel is kept constant (30 µL). Scale bar is 5 mm. B) Constant Volume average wicking distances measured from the top of the inlet. N=6. Data is displayed as mean ± standard deviation.

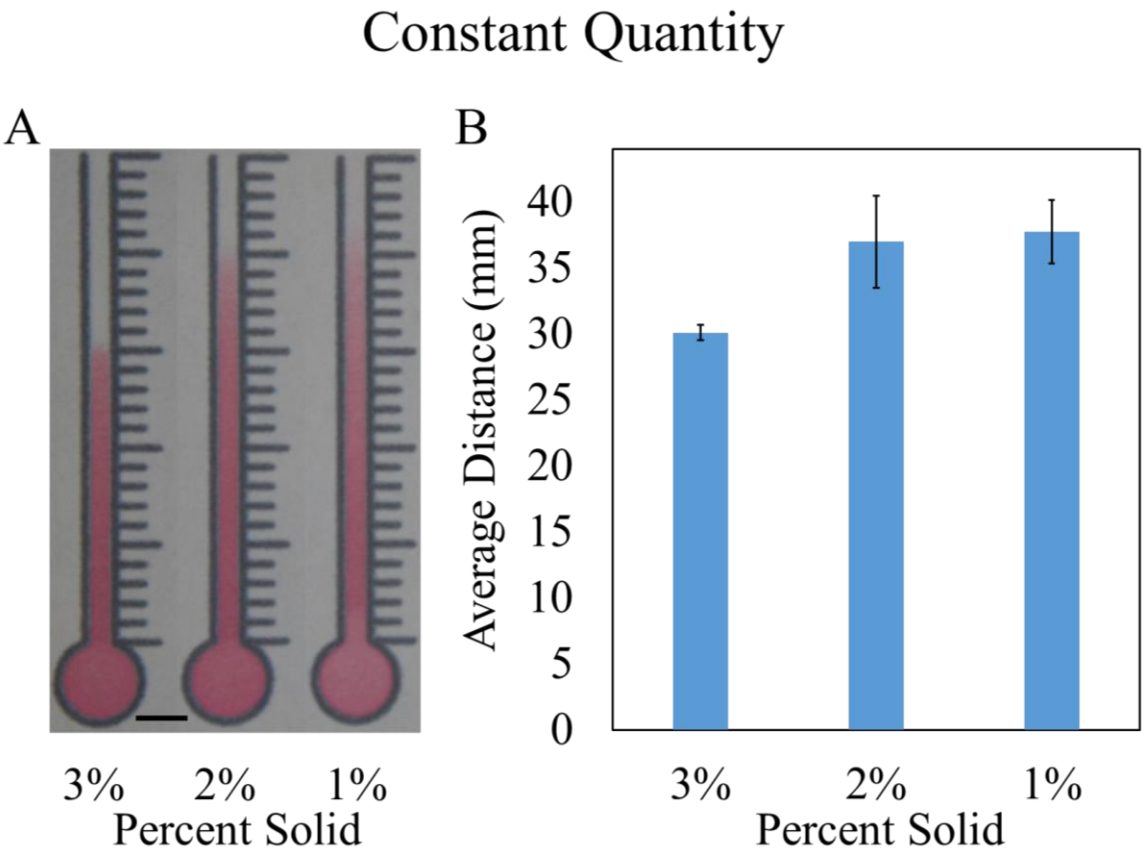

Figure 4-7. Microsphere Solution Optimizations - Constant Quantity. A) Wicking distances of 1-3% solid microspheres in the paper channels when the quantity of microspheres in each channel is kept constant. Scale bar is 5 mm. B) Constant Quantity average wicking distances measured from the top of the inlet. N=4. Data is displayed as mean ± standard deviation.

Surfactant Concentration

The presence of small amounts of a surfactant can significantly increase the distance wicked by the microspheres. At high concentrations (>1%) of Tween-20, microsphere solutions were able to penetrate the wax boundaries of the channel, resulting in dramatically reduced wicking distances. Solutions containing low (<0.1%) or no surfactant resulted in microspheres that did not travel very far. However, within those bounds, the microspheres

are able to wick much further (Fig. 4-8). In all subsequent experiments, a Tween-20 concentration of 0.1% was used to minimize the potential for leakage while maximizing wicking distances.

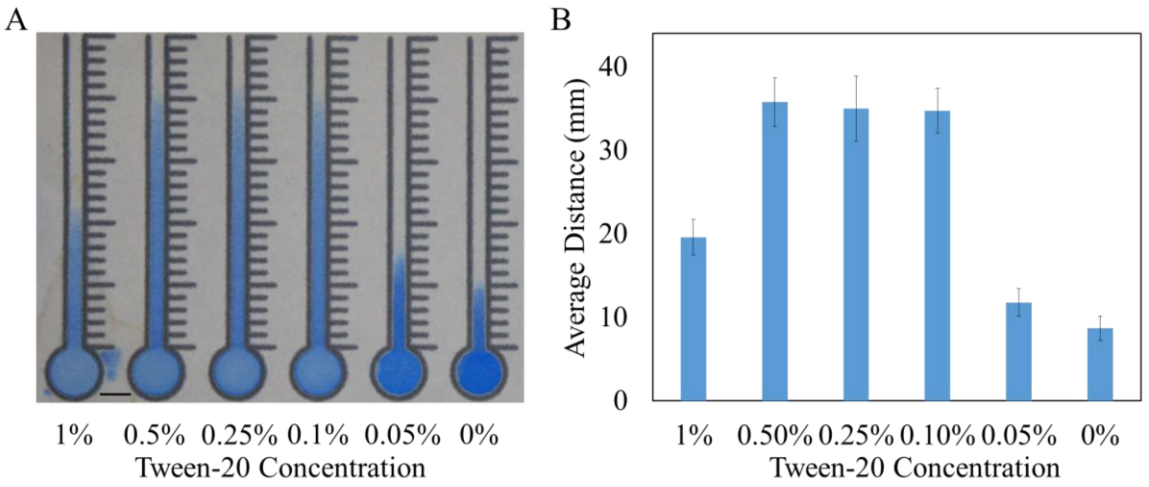

Figure 4-8. Microsphere Solution Optimizations - Surfactant Concentration. A) Wicking distances of 2% solid microspheres in Whatman grade 4 filter paper in solutions containing different Tween-20 concentrations. Scale bar is 5 mm. B) Surfactant optimization average wicking distances measured from the top of the inlet. N=10. Data is displayed as mean ± standard deviation.

Target Concentration Dependent Wicking

As a demonstration of the viability of this detection mechanism to quantify ssDNA, microspheres conjugated with Probe A and Probe B were mixed with a target strand, an oligomer partially complementary to both probes (A'-B') (Fig. 4-9). At lower target concentrations (10 nM - 1 µM), the distance wicked by the microspheres was inversely proportional to the target concentration (shorter distances at higher concentrations), while at higher concentrations (>1 µM), the distance traveled was proportional to the target concentration (longer distances at higher concentrations). When mixed with oligomers

only complementary to one (Strand C), or to neither (Strand D) probe, the microspheres failed to aggregate and displayed nearly identical wicking behavior to microspheres mixed with only H_2O, suggesting that the aggregation is hybridization-induced.

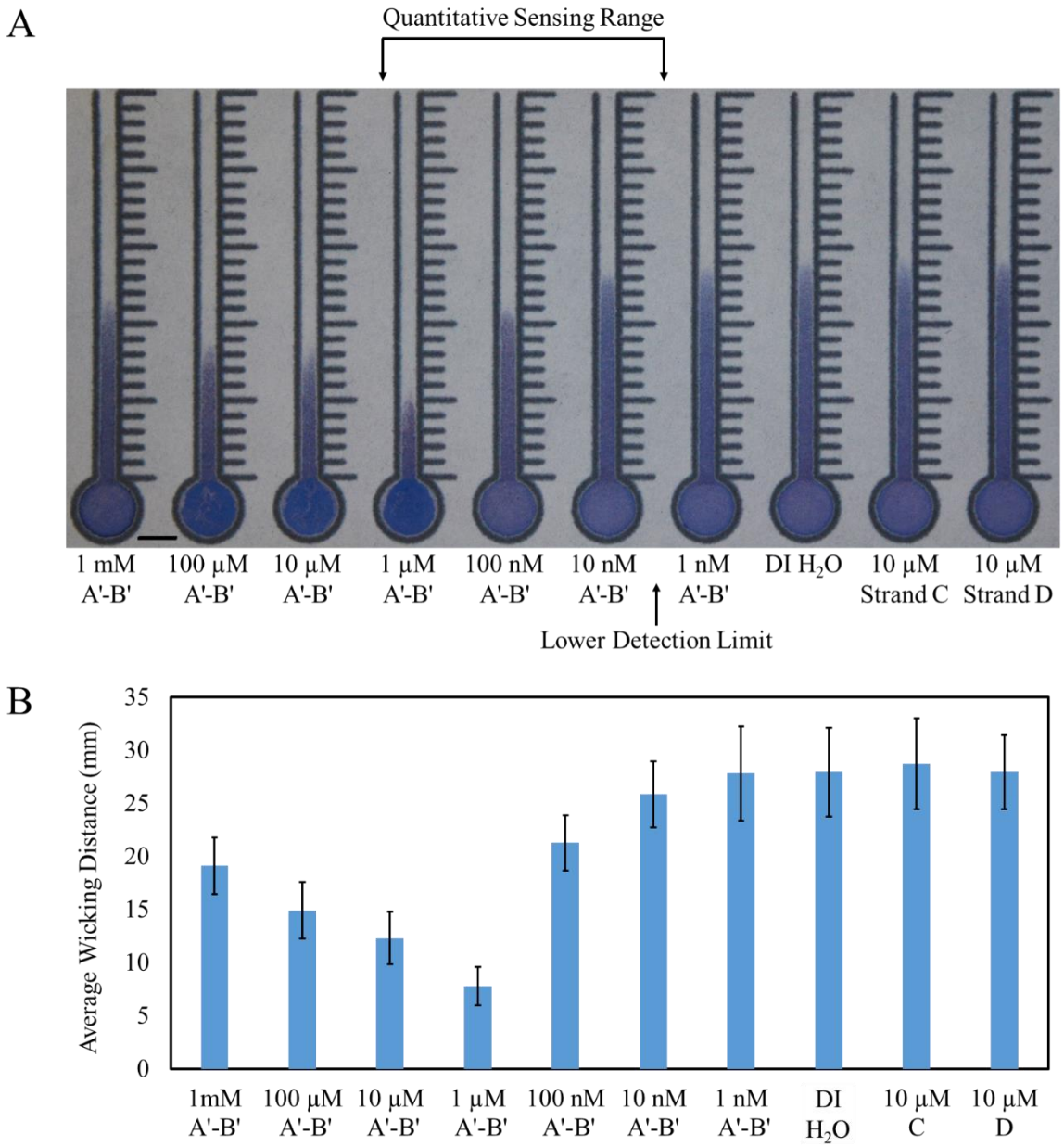

Figure 4-9. Target Concentration Dependent Wicking. A) Wicking distances of 2% solid microsphere solutions in the paper channels. Seven different A'-B' linker concentrations were tested, ranging from 1 nM - 1 mM, along with a DI H_2O control, and 10 µM strands C and D. A'-B' is partially complementary to both probes A and B, while strand C is partially complementary to only probe A and strand D is not complementary to either probe. 30 µL of 2% solid microspheres solution (equal parts Strand A-conjugated microspheres, Strand B-conjugated microspheres, and linker strand) deposited in the inlet of each channel after 30 min incubation at 45°C. Scale bar is 5 mm. B) Average wicking distances measured from the top of the inlet. Data is displayed as mean ± standard deviation. N=30.

The inversely proportional range (10 nM – 1 µM) is considered the quantitative sensing range, as the difference in distances traveled by the microspheres at each target strand concentration are much larger than of those in the proportional region, as shown in Figure 4-9. The proportional wicking behavior at high linker concentrations is thought to be caused by excess target strands hybridizing to each available probe, preventing aggregates from forming (Fig. 4-10).

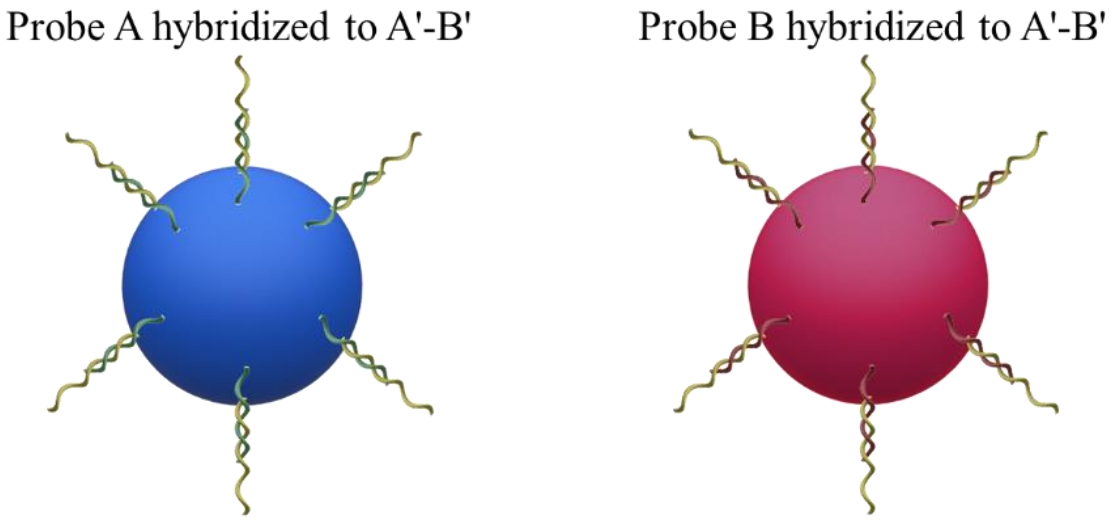

Figure 4-10. Hypothesized mechanism for high concentration wicking behavior. Target strands (yellow) can bind to every available probe (red and green), preventing 3-strand complexes from forming.

Aggregate Formation

In order to optimize the incubation step, a thorough understanding of microsphere aggregate formation is needed. To this end, microsphere mixtures were prepared as described above and then, at various time intervals, 1 µL samples were withdrawn and deposited into the aggregate observation wells and observed under a microscope. The size

and growth of the microsphere aggregates are displayed in a series of violin plots in Figure 4-11. In these violin plots, the x-axis of the violin plot is time, and the y-axis shows the projected area of the aggregates. The width of each violin represents the probability density of that size. The interquartile range is indicated inside each violin as well.

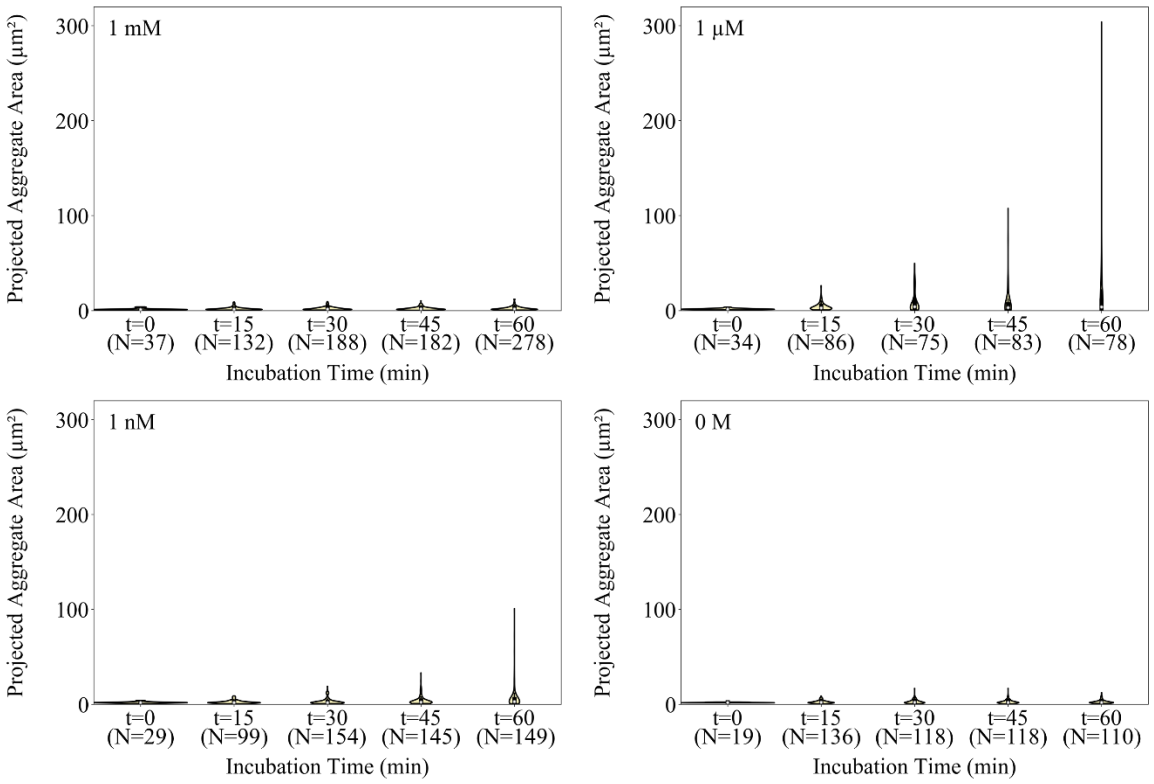

Figure 4-11. Aggregate size (projected area) distributions of microspheres mixed with 1 mM, 1µM, 1 nM, and 0 M A'-B' with varying incubation times in 15 minute intervals. Five images for each time point and each concentration were analyzed. Aggregate counts (N) for each condition are listed below the corresponding time point. The counts for the t=0 conditions were low due to the microspheres being highly dispersed and nearly all appeared as individual microspheres.

The microspheres mixed with 1 nM target formed aggregates gradually and after 60 min, a large fraction of the aggregate population remained small. This matches the previous wicking data that showed microspheres mixed with 1 nM target wicked the same distance

as the 0 M control. Microspheres mixed with 1 µM target, on the other hand, formed aggregates immediately and by 60 min, nearly all of the microspheres were bound in aggregates. The largest aggregates were over 300 μm^2. The 1 mM target microspheres formed rather small aggregates and the overall size and distribution did not change after 15 min. This seems to support the explanation that high target concentrations rapidly saturate microsphere surfaces with target strands, allowing only a short time interval for aggregate formation (Fig. 4-10).

To confirm that the microspheres were hybridizing with their complementary microspheres, aggregates made with red and green fluorescent microspheres were examined under the microscope. Figure 4-12 depicts the aggregates of fluorescent microspheres with brightfield and composite red/green fluorescent filters for 1 mM, 1 µM, 1 nM, and 0 M target concentrations.

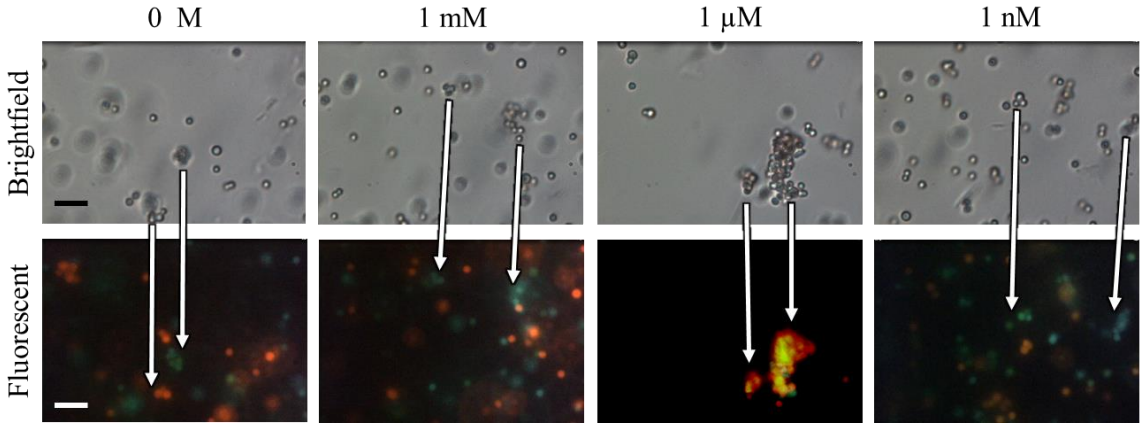

Figure 4-12. Microsphere Aggregate Composition. Brightfield and composite fluorescent images of 1µm red and green microspheres mixed with 1 mM, 1 µM, 1 nM, and 0 M A'-B' after 60 minute incubation. Scale bars are 5 µm. Arrows indicate the movement of individual aggregates during the time interval between the brightfield and fluorescent images.

In order to verify that the large aggregates only form from mixtures of the two populations of microspheres, each probe was tested separately. The single strands were first tested with DI water, and then tested with 1 µM A'-B' (Fig. 4-13). While some small aggregates did form, the aggregates were comprised of few microspheres and looked broadly similar the microspheres mixed with DI H_2O.

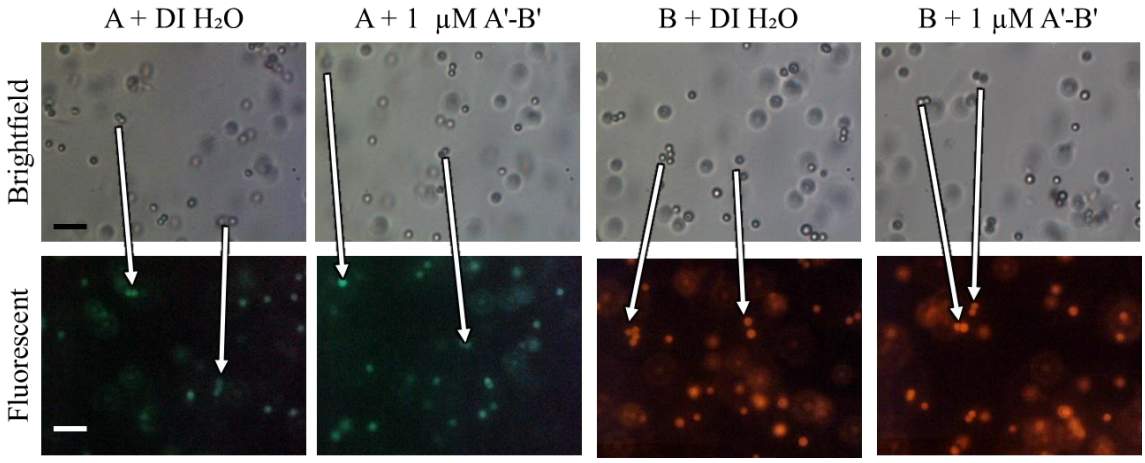

Figure 4-13. Microsphere Single Color Aggregates. Brightfield and fluorescent images of single-color microspheres mixed with either 1 µM A'-B' or DI H2O after 60 minute incubation. Scale bars are 5 µm. Arrows indicate the movement of individual aggregates during the time interval between the brightfield and fluorescent images.

Spiked Plant Extract Detection

Detection of Target ssDNA in Post-Extraction Spike

Aliquots of DNA extracted from the sour orange leaves were spiked with A'-B' resulting in concentrations ranging from 1 nM to 100 µM. These solutions where then mixed with the microspheres as described above. The wicking behavior of the spiked mixtures performed broadly similar to those mixed with A'-B' in water, however, with overall shorter wicking distances (Fig. 4-14). The shorter distances are likely due to the higher viscosity

of the re-solubilized DNA. Diluting the extracts would likely solve this issue, but may reduce sensitivity.

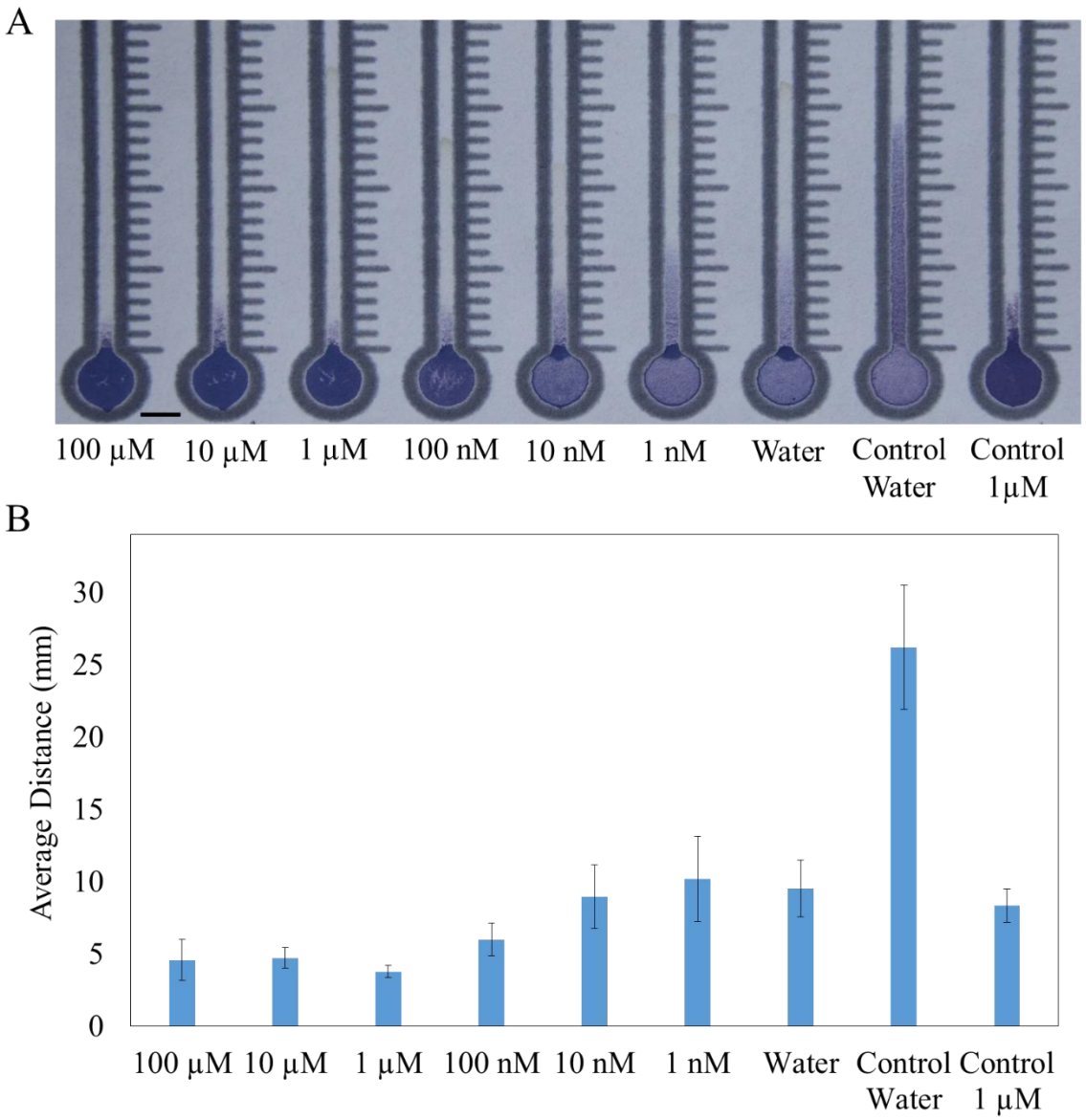

Figure 4-14. Target Concentration Dependent Wicking in Extracted Plant DNA. A) Wicking distances of 2% solid microsphere solutions in the paper channels. DNA extracts from sour orange leaves were spiked with six different A'-B' linker concentrations, ranging from 1 nM - 100 µM, along with a DI H2O control. Two more controls were tested with microspheres mixed with 1 µM and 0 M A'-B' in water. Scale bar is 5 mm. B) Average wicking distances measured from the top of the inlet. N=4. Data is displayed as mean ± standard deviation.

Detection of Target ssDNA in Pre-Extraction Spike

As a proof of concept of detecting a DNA strand present in the leaf sample before extraction, ground leaf tissue was spiked with A'-B' before the extraction, enough to result in a nominal concentration of 1 µM. As depicted in Fig 4-15, the microspheres mixed with the spiked extract wicked a shorter distance than the unspiked control. While the distances traveled by the spiked sample does not match the distance traveled by the 1 µM post-extraction spiked microspheres, the extraction process is not lossless. The distance traveled does seem to correspond though to an A'-B' concentration of between 10-100 nM.

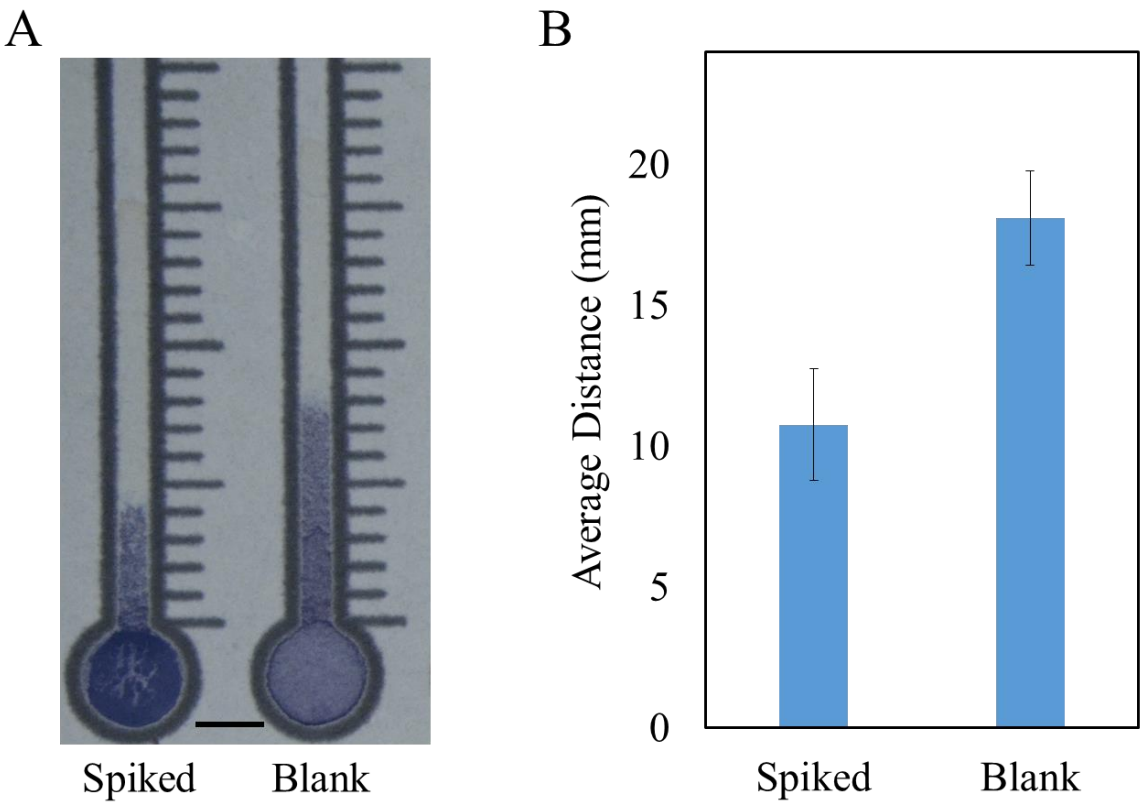

Figure 4-15. Qualitative Target Detection in Extracted Plant DNA. A) Wicking distances of 2% solid microsphere solutions in the paper channels. Sour orange leaves were spiked with 10 µL of 10 µM A'-B' before extraction, resulting in a nominal post-extraction concentration of 1µM. B) Average wicking distances measured from the top of the inlet. N=3. Data is displayed as mean ± standard deviation. Scale bar is 5 mm.

Travel to Uganda

In the summer of 2018, I traveled to Gulu, Uganda to meet with our collaborators from Gulu University (Fig. 4-16) to test the device on samples of sweet potatoes infected with Sweet Potato Feathery Mottle Virus (SPFMV). SPFMV is one of the two viruses that contributed to Sweet Potato Virus Disease, a devastating disease that results in significant crop loss. DNA probes were designed and adapted from exisiting PCR primers (Table 4-2).[83] SPFMV is a ssRNA virus and the PCR primers result in an amplicon 703 bp long. The total length of the genome is approximately 11 kbp long, much longer than the A'-B' strands used previously. As the initial tests with microspheres conjugated with SPFMV Probes 1 and 2 were unsuccessful, the full RNA extract was digested using RNAse H and custom designed DNA conjugates. RNAse H is an enzyme that only breaks down RNA that has hybridized to DNA, so when the conjugates are mixed with the extracted RNA, the RNAse H digestion releases fragments of ssRNA whose ends are exactly complementary to SPFMV Probes 1 and 2. Initial attempts resulted in total digestion of all RNA content into single nucleotides, so further work is warranted to refine the detection method.

In conclusion, microspheres, when conjugated to appropriately complementary probes rapidly form aggregates in the presence of the target. By depositing these aggregates onto paper, the degree of aggregation can be quantified via the overall distance traveled by the microspheres. Larger aggregates, formed in relatively high concentrations of the target strand result in the shortest wicking distances, due to the inability of the large aggregates to fit through the paper's pores and due to an overall reduction in the quantity of discrete

microsphere particles in solution. This length can then be calibrated to determine the concentration of the targeted DNA strand.

In this work, we successfully demonstrated the quantitative, distance-based detection of ssDNA in buffer, as well as in extracted plant DNA spiked after extraction with a target ssDNA strand in a paper-based microfluidic device. Further, we demonstrated the qualitative detection of a target ssDNA strand added to plant tissue before DNA extraction. With further calibration, quantitative detection will also be possible.

Figure 4-17. Photos from Gulu, Uganda. A) Dr. Richard Echodu and Brent Kalish. B) Mr. Hilary Edema and Brent Kalish gathering infected sweet potato samples for testing.

Table 4-2: Sweet Potato Feathery Mottle Virus Probes and Conjugates

Name	**Sequence**
Probe 1[83]	5'-/5AmMC6//iSp18/TTT TTTT TTT T TC TTC TTG CGT GGA GAC GT-3'
Probe 2[83]	5'-TTG CTA GTG TCT CGT CCT TTT TTT TTT/iSp18//3AmMO/-3'
5' RNAse H conjugate	5'-ATA TGA TTC TGG AAT GGT TG-3'
3' RNAse H conjugate	5'-GTC GTG TGC CTC TCC GTA TC-3'

Chapter 5: Conclusions

Research Conclusions

Overall, laser-etching was found to be an effective and simple method of enhancing or inhibiting wicking speeds in paper microfluidic channels. In a single manufacturing step, the channels can be patterned and etched, resulting in a versatility of design, where devices with identical channels can have different mixing and delivery timings based on the degree of etching within a channel. This behavior was successfully demonstrated in a simple, three channel mixer. In untaped channels, moderate etching provided slight wicking speed enhancements (2-10%), while the heaviest etching slowed wicking by nearly 20%. Taped channels, on the other hand, experienced consistent speed increases as the level of etching increased, with the most heavily etched channels wicking nearly 70% faster than unetched channels. While no clear dependence upon wicking angle was observed, horizontal wicking in untapped channels seemed to have their performance depend heavily on how liquid was delivered, particularly in the most heavily etched channels – the ones with the most significantly modified surfaces – suggesting that tape-sealed channels are likely to preferred as a means to minimize user-variability when depositing a sample.

In the development of the quantitative DNA detection device, several factors that affect the overall distance travelled by the microspheres were investigated, such as microsphere concentration, surfactant concentration, and the total deposited mixture volume. Further, the specifics of aggregate formation were studied to determine how quickly aggregates grow and what proportion of the total microsphere population are eventually bound into aggregates, in order to strike the optimal balance between minimizing overall testing time and maximizing wicking distance differences. This

resulted in the choice of a 30 minutes incubation at 45°C, as aggregates formed from the different concentrations of linker were already significantly different sizes. Finally, the quantitative detection of a mock target ssDNA strand was demonstrated in buffer and in extracted plant DNA spiked with the target strand post extraction. Qualitative detection was also demonstrated with the same mock target strand spiked into the plant material pre-extraction.

Suggested Future Directions

Etched Wicking

The work detailed in this dissertation focuses on the effect the laser etching had on the speed at which DI H_2O wicked through Whatman 1 Chromatography paper. However, in microfluidic devices, the wicking fluids are often much more complex matrices, with solutions containing a variety of biological targets of interest, such as proteins and nucleic acids. The highly porous etched surface of the paper may affect the transport of these targets, as the increased surface area may promote increased non-specific binding.

Microsphere Aggregate Formation

While the device as detailed above has a detection range from 1 nM to 1 µM, varying the microsphere mixture incubation temperatures and cooling strategies may provide for an expanded detection range. For the set of experiments depicted in Figure 4-14, the microspheres were incubated at 45°C, a few degrees below the melting temperature of the probes. However, when incubated at 50°C, the microsphere mixtures did not result in the 1 µM channel wicking the shortest distance. Instead, the highest concentrations

wicked the shortest distance, preserving the inversely proportional behavior over the entire range, resulting in an expanded detection range (Fig. 5-1). Further investigation regarding both incubation and cooling times are warranted to maximize sensitivity.

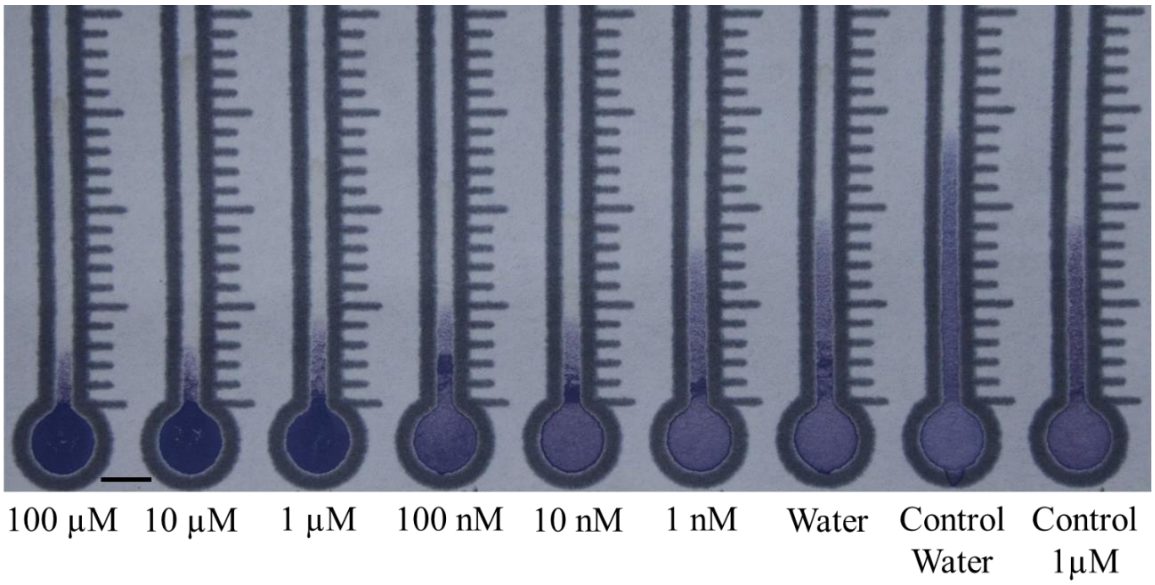

Figure 5-1. Target Concentration Dependent Wicking with Elevated Incubation Temperature. Microspheres mixed with DNA extract from sour orange leaves spiked with A'-B' incubated at 50°C for 30 minutes before deposition. The highest concentrations wicked the shortest distances. The control channels contain microspheres mixed with water or A'-B' in water instead of spiked plant extract. Scale bar is 5 mm.

Matrix effects of Extracted DNA/RNA

Just as the concentration of surfactant contributed to the distance that microspheres were able to wick through the paper, so too can contaminants in the extracted nucleotides. The viscosity of the extract can play a significant role in overall microsphere wicking distances. Some plants' extracts may require considerable dilution to allow the microspheres to wick freely; further optimization will be necessary to maintain low limits of detection under those conditions.

Humidity and Temperature wicking sensitivity

The ambient humidity and temperature in which a paper device is wicking can have significant effects on its overall wicking performance.[60] With the limited sample volume deposited containing the microsphere solution, excessive evaporation may reduce the volume of liquid available to wick, increasing the overall microsphere concentration and thus reducing the maximum wicking distance. Future researchers would do well to ensure their device is optimized for the expected ambient conditions or ensure that the device is appropriately sealed.

REFERENCES

1. V. Gubala, L. F. Harris, A. J. Ricco, M. X. Tan and D. E. Williams, "Point of care diagnostics: status and future", *Anal Chem*, 2012, **84**, 487.

2. X. Li, D. R. Ballerini and W. Shen, "A perspective on paper-based microfluidics: Current status and future trends", *Biomicrofluidics*, 2012, **6**, 11301.

3. D. M. Cate, J. A. Adkins, J. Mettakoonpitak and C. S. Henry, "Recent developments in paper-based microfluidic devices", *Analytical Chemistry*, 2015, **87**, 19.

4. E. Fu, "Enabling robust quantitative readout in an equipment-free model of device development", *Analyst*, 2014, **139**, 4750.

5. H. Kettler, K. White and S. Hawkes, *Mapping the landscape of diagnostics for sexually transmitted infections*, World Health Organization, Geneva, SW, 2004.

6. H. Yagoda, "Applications of Confined Spot Tests in Analytical Chemistry: Preliminary Paper", *Industrial & Engineering Chemistry Analytical Edition*, 1937, **9**, 79.

7. R. H. Muller, "Instrumentation in Microanalysis", *Anal Chem*, 1949, **21**, 427.

8. X. Li, J. Tian and W. Shen, "Progress in patterned paper sizing for fabrication of paper-based microfluidic sensors", *Cellulose*, 2010, **17**, 649.

9. X. Li, J. Tian, G. Garnier and W. Shen, "Fabrication of paper-based microfluidic sensors by printing", *Colloids and Surfaces B: Biointerfaces*, 2010, **76**, 564.

10. J. Olkkonen, K. Lehtinen and T. Erho, "Flexographically Printed Fluidic Structures in Paper", *Analytical Chemistry*, 2010, **82**, 10246.

11. W. Dungchai, O. Chailapakul and C. S. Henry, "A low-cost, simple, and rapid fabrication method for paper-based microfluidics using wax screen-printing", *Analyst*, 2011, **136**, 77.

12. E. Carrilho, A. W. Martinez and G. M. Whitesides, "Understanding wax printing: a simple micropatterning process for paper-based microfluidics", *Anal Chem*, 2009, **81**, 7091.

13. Y. Lu, W. W. Shi, J. H. Qin and B. C. Lin, "Fabrication and Characterization of Paper-Based Microfluidics Prepared in Nitrocellulose Membrane By Wax Printing", *Analytical Chemistry*, 2010, **82**, 329.

14. I. Jang and S. Song, "Facile and precise flow control for a paper-based microfluidic device through varying paper permeability", *Lab on a Chip*, 2015, **15**, 3405.

15. S. G. Jeong, S. H. Lee, C. H. Choi, J. Kim and C. S. Lee, "Toward instrument-free digital measurements: a three-dimensional microfluidic device fabricated in a single sheet of paper by double-sided printing and lamination", *Lab on a Chip*, 2015, **15**, 1188.

16. A. W. Martinez, S. T. Phillips, M. J. Butte and G. M. Whitesides, "Patterned paper as a platform for inexpensive, low-volume, portable bioassays", *Angew Chem Int Ed Engl*, 2007, **46**, 1318.

17. A. W. Martinez, S. T. Phillips, B. J. Wiley, M. Gupta and G. M. Whitesides, "FLASH: A rapid method for prototyping paper-based microfluidic devices", *Lab on a Chip*, 2008, **8**, 2146.

18. K. Abe, K. Kotera, K. Suzuki and D. Citterio, "Inkjet-printed paperfluidic immuno-chemical sensing device", *Analytical and Bioanalytical Chemistry*, 2010, **398**, 885.

19. K. Abe, K. Suzuki and D. Citterio, "Inkjet-Printed Microfluidic Multianalyte Chemical Sensing Paper", *Analytical Chemistry*, 2008, **80**, 6928.

20. G. Chitnis, Z. Ding, C.-L. Chang, C. A. Savran and B. Ziaie, "Laser-treated hydrophobic paper: an inexpensive microfluidic platform", *Lab on a Chip*, 2011, **11**, 1161.

21. X. Li, J. F. Tian, T. Nguyen and W. Shen, "Paper-Based Microfluidic Devices by Plasma Treatment", *Analytical Chemistry*, 2008, **80**, 9131.

22. P. K. Kao and C. C. Hsu, "One-step rapid fabrication of paper-based microfluidic devices using fluorocarbon plasma polymerization", *Microfluidics and Nanofluidics*, 2014, **16**, 811.

23. C. L. Cassano and Z. H. Fan, "Laminated paper-based analytical devices (LPAD): fabrication, characterization, and assays", *Microfluidics and Nanofluidics*, 2013, **15**, 173.

24. E. M. Fenton, M. R. Mascarenas, G. P. López and S. S. Sibbett, "Multiplex Lateral-Flow Test Strips Fabricated by Two-Dimensional Shaping", *ACS Applied Materials & Interfaces*, 2009, **1**, 124.

25. J. F. Nie, Y. Z. Liang, Y. Zhang, S. W. Le, D. N. Li and S. B. Zhang, "One-step patterning of hollow microstructures in paper by laser cutting to create microfluidic analytical devices", *Analyst*, 2013, **138**, 671.

26. E. Fu, S. A. Ramsey, P. Kauffman, B. Lutz and P. Yager, "Transport in two-dimensional paper networks", *Microfluid Nanofluidics*, 2011, **10**, 29.

27. E. Fu, P. Kauffman, B. Lutz and P. Yager, "Chemical signal amplification in two-dimensional paper networks", *Sensors and Actuators, B: Chemical*, 2010, **149**, 325.

28. E. Evans, E. F. M. Gabriel, W. K. T. Coltro and C. D. Garcia, "Rational selection of substrates to improve color intensity and uniformity on microfluidic paper-based analytical devices", *Analyst*, 2014, **139**, 2127.

29. A. K. Yetisen, M. S. Akram and C. R. Lowe, "Paper-based microfluidic point-of-care diagnostic devices", *Lab on a Chip*, 2013, **13**, 2210.

30. C. Danks and I. Barker, "On-site detection of plant pathogens using lateral-flow devices*", *EPPO Bulletin*, 2000, **30**, 421.

31. D. Y. Stevens, C. R. Petri, J. L. Osborn, P. Spicar-Mihalic, K. G. McKenzie and P. Yager, "Enabling a microfluidic immunoassay for the developing world by integration of on-card dry reagent storage", *Lab on a Chip*, 2008, **8**, 2038.

32. D. M. Cate, W. Dungchai, J. C. Cunningham, J. Volckens and C. S. Henry, "Simple, distance-based measurement for paper analytical devices", *Lab on a Chip*, 2013, **13**, 2397.

33. R. Chen, H. Li, H. Zhang, S. Zhang, W. Shi, J. Shen and Z. Wang, "Development of a lateral flow fluorescent microsphere immunoassay for the determination of sulfamethazine in milk", *Analytical and Bioanalytical Chemistry*, 2013, **405**, 6783.

34. W. Chen, X. Fang, H. Li, H. Cao and J. Kong, "A Simple Paper-Based Colorimetric Device for Rapid Mercury(II) Assay", *Scientific Reports*, 2016, **6**, 31948.

35. Y. Song, P. Gyarmati, A. C. Araujo, J. Lundeberg, H. Brumer, 3rd and P. L. Stahl, "Visual detection of DNA on paper chips", *Analytical Chemistry*, 2014, **86**, 1575.

36. W. Dungchai, O. Chailapakul and C. S. Henry, "Electrochemical Detection for Paper-Based Microfluidics", *Analytical Chemistry*, 2009, **81**, 5821.

37. M. Pozuelo, P. Blondeau, M. Novell, F. J. Andrade, F. Xavier Rius and J. Riu, "Paper-based chemiresistor for detection of ultralow concentrations of protein", *Biosensors and Bioelectronics*, 2013, **49**, 462.

38. A. Nilghaz, D. R. Ballerini, X. Y. Fang and W. Shen, "Semiquantitative analysis on microfluidic thread-based analytical devices by ruler", *Sensors and Actuators B-Chemical*, 2014, **191**, 586.

39. W. Dungchai, Y. Sameenoi, O. Chailapakul, J. Volckens and C. S. Henry, "Determination of aerosol oxidative activity using silver nanoparticle aggregation on paper-based analytical devices", *Analyst*, 2013, **138**, 6766.

40. R. F. Zuk, V. K. Ginsberg, T. Houts, J. Rabbie, H. Merrick, E. F. Ullman, M. M. Fischer, C. C. Sizto, S. N. Stiso and D. J. Litman, "Enzyme Immunochromatography - a Quantitative Immunoassay Requiring No Instrumentation", *Clinical chemistry*, 1985, **31**, 1144.

41. V. Y. S. Liu, T. Y. Lin, W. Schrier, M. Allen and P. Singh, "Accumeter(R) Noninstrumented Quantitative Assay of High-Density-Lipoprotein in Whole-Blood", *Clinical chemistry*, 1993, **39**, 1948.

42. Y. Zhang, C. B. Zhou, J. F. Nie, S. W. Le, Q. Qin, F. Liu, Y. P. Li and J. P. Li, "Equipment-Free Quantitative Measurement for Microfluidic Paper-Based Analytical Devices Fabricated Using the Principles of Movable-Type Printing", *Analytical Chemistry*, 2014, **86**, 2005.

43. G. G. Lewis, M. J. DiTucci and S. T. Phillips, "Quantifying Analytes in Paper-Based Microfluidic Devices Without Using External Electronic Readers", *Angewandte Chemie International Edition*, 2012, **51**, 12707.

44. W. Leung, C. P. Chan, T. H. Rainer, M. Ip, G. W. H. Cautherley and R. Renneberg, "InfectCheck CRP barcode-style lateral flow assay for semi-quantitative detection of C-reactive protein in distinguishing between bacterial and viral infections", *Journal of Immunological Methods*, 2008, **336**, 30.

45. K.-K. Fung, C. P.-Y. Chan and R. Renneberg, "Development of enzyme-based bar code-style lateral-flow assay for hydrogen peroxide determination", *Analytica Chimica Acta*, 2009, **634**, 89.

46. L. F. Cai, Y. L. Fang, Y. H. Mo, Y. S. Huang, C. X. Xu, Z. Zhang and M. X. Wang, "Visual quantification of Hg on a microfluidic paper-based analytical device using distance-based detection technique", *AIP Advances*, 2017, **7**.

47. K. Yamada, D. Citterio and C. S. Henry, ""Dip-and-read" paper-based analytical devices using distance-based detection with color screening", *Lab on a Chip*, 2018, **18**, 1485.

48. C. T. Gerold, E. Bakker and C. S. Henry, "Selective Distance-Based K+ Quantification on Paper-Based Microfluidics", *Analytical Chemistry*, 2018, **90**, 4894.

49. X. F. Wei, T. Tian, S. S. Jia, Z. Zhu, Y. L. Ma, J. J. Sun, Z. Y. Lin and C. J. Yang, "Microfluidic Distance Readout Sweet Hydrogel Integrated Paper Based Analytical Device (mu DiSH-PAD) for Visual Quantitative Point-of-Care Testing", *Analytical Chemistry*, 2016, **88**, 2345.

50. I. Hongwarittorrn, N. Chaichanawongsaroj and W. Laiwattanapaisal, "Semi-quantitative visual detection of loop mediated isothermal amplification (LAMP)-generated DNA by distance-based measurement on a paper device", *Talanta*, 2017, **175**, 135.

51. H. Shibata, Y. Hiruta and D. Citterio, "Fully inkjet-printed distance-based paper microfluidic devices for colorimetric calcium determination using ion-selective optodes", *Analyst*, 2019, **144**, 1178.

52. A. Z. Qamar, G. Parker, G. R. Kinsel and M. H. Shamsi, "Evolution of wax-on-plastic microfluidics for sub-microliter flow dynamics and its application in distance-based assay", *Microfluidics and Nanofluidics*, 2019, **23**.

53. H. Li, D. Han, G. M. Pauletti and A. J. Steckl, "Blood coagulation screening using a paper-based microfluidic lateral flow device", *Lab on a Chip*, 2014, **14**, 4035.

54. S.-G. Jeong, J. Kim, S. H. Jin, K.-S. Park and C.-S. Lee, "Flow control in paper-based microfluidic device for automatic multistep assays: A focused minireview", *Korean Journal of Chemical Engineering*, 2016, **33**, 2761.

55. E. Fu and C. Downs, "Progress in the development and integration of fluid flow control tools in paper microfluidics", *Lab on a Chip*, 2017, **17**, 614.

56. J. C. Cunningham, P. R. DeGregory and R. M. Crooks, "New Functionalities for Paper-Based Sensors Lead to Simplified User Operation, Lower Limits of Detection, and New Applications", *Annu Rev Anal Chem (Palo Alto Calif)*, 2016, **9**, 183.

57. X. Jiang and Z. H. Fan, "Fabrication and Operation of Paper-Based Analytical Devices", *Annu Rev Anal Chem (Palo Alto Calif)*, 2016, **9**, 203.

58. E. W. Washburn, "The Dynamics of Capillary Flow", *Physical Review*, 1921, **17**, 273.

59. R. Lucas, "Ueber das Zeitgesetz des kapillaren Aufstiegs von Flüssigkeiten", *Kolloid-Zeitschrift*, 1918, **23**, 15.

60. C. Castro, C. Rosillo and H. Tsutsui, "Characterizing effects of humidity and channel size on imbibition in paper-based microfluidic channels", *Microfluidics and Nanofluidics*, 2017, **21**, 21.

61. S. Mendez, E. M. Fenton, G. R. Gallegos, D. N. Petsev, S. S. Sibbett, H. A. Stone, Y. Zhang and G. P. Lopez, "Imbibition in porous membranes of complex shape: quasi-stationary flow in thin rectangular segments", *Langmuir*, 2010, **26**, 1380.

62. E. Elizalde, R. Urteaga and C. L. Berli, "Rational design of capillary-driven flows for paper-based microfluidics", *Lab on a Chip*, 2015, **15**, 2173.

63. D. Shou and J. Fan, "Structural optimization of porous media for fast and controlled capillary flows", *Phys Rev E Stat Nonlin Soft Matter Phys*, 2015, **91**, 053021.

64. E. Fu, B. Lutz, P. Kauffman and P. Yager, "Controlled reagent transport in disposable 2D paper networks", *Lab on a Chip*, 2010, **10**, 918.

65. A. Apilux, Y. Ukita, M. Chikae, O. Chailapakul and Y. Takamura, "Development of automated paper-based devices for sequential multistep sandwich enzyme-linked immunosorbent assays using inkjet printing", *Lab on a Chip*, 2013, **13**, 126.

66. B. J. Toley, B. McKenzie, T. Liang, J. R. Buser, P. Yager and E. Fu, "Tunable-Delay Shunts for Paper Micro fl uidic Devices", *Analytical Chemistry*, 2013, **85**, 11545.

67. B. Lutz, T. Liang, E. Fu, S. Ramachandran, P. Kauffman and P. Yager, "Dissolvable fluidic time delays for programming multi-step assays in instrument-free paper diagnostics", *Lab on a Chip*, 2013, **13**, 2840.

68. S. Jahanshahi-Anbuhi, A. Henry, V. Leung, C. Sicard, K. Pennings, R. Pelton, J. D. Brennan and C. D. Filipe, "Paper-based microfluidics with an erodible polymeric bridge giving controlled release and timed flow shutoff", *Lab on a Chip*, 2014, **14**, 229.

69. P. J. He, I. N. Katis, R. W. Eason and C. L. Sones, "Engineering fluidic delays in paper-based devices using laser direct-writing", *Lab on a Chip*, 2015, **15**, 4054.

70. C. H. Weng, M. Y. Chen, C. H. Shen and R. J. Yang, "Colored wax-printed timers for two-dimensional and three-dimensional assays on paper-based devices", *Biomicrofluidics*, 2014, **8**, 066502.

71. J. H. Shin, J. Park, S. H. Kim and J. K. Park, "Programmed sample delivery on a pressurized paper", *Biomicrofluidics*, 2014, **8**, 054121.

72. E. T. da Silva, M. Santhiago, F. R. de Souza, W. K. Coltro and L. T. Kubota, "Triboelectric effect as a new strategy for sealing and controlling the flow in paper-based devices", *Lab on a Chip*, 2015, **15**, 1651.

73. S. Jahanshahi-Anbuhi, P. Chavan, C. Sicard, V. Leung, S. M. Hossain, R. Pelton, J. D. Brennan and C. D. Filipe, "Creating fast flow channels in paper fluidic devices to control timing of sequential reactions", *Lab on a Chip*, 2012, **12**, 5079.

74. C. K. Camplisson, K. M. Schilling, W. L. Pedrotti, H. A. Stone and A. W. Martinez, "Two-ply channels for faster wicking in paper-based microfluidic devices", *Lab on a Chip*, 2015, **15**, 4461.

75. D. L. Giokas, G. Z. Tsogas and A. G. Vlessidis, "Programming fluid transport in paper-based microfluidic devices using razor-crafted open channels", *Anal Chem*, 2014, **86**, 6202.

76. A. C. Glavan, R. V. Martinez, E. J. Maxwell, A. B. Subramaniam, R. M. D. Nunes, S. Soh and G. M. Whitesides, "Rapid fabrication of pressure-driven open-channel microfluidic devices in omniphobic RF paper", *Lab on a Chip*, 2013, **13**, 2922.

77. C. Renault, X. Li, S. E. Fosdick and R. M. Crooks, "Hollow-channel paper analytical devices", *Anal Chem*, 2013, **85**, 7976.

78. J.-H. Shin, G.-J. Lee, W. Kim and S. Choi, "A stand-alone pressure-driven 3D microfluidic chemical sensing analytic device", *Sensors and Actuators B: Chemical*, 2016, **230**, 380.

79. B. Kalish and H. Tsutsui, "Patterned adhesive enables construction of nonplanar three-dimensional paper microfluidic circuits", *Lab on a Chip*, 2014, **14**, 4354.

80. B. Kalish and H. Tsutsui, "Using Adhesive Patterning to Construct 3D Paper Microfluidic Devices", *J Vis Exp*, 2016, e53805.

81. B. Kalish, J. Luong, J. Roper, C. Beaudette and H. Tsutsui, Distance-based quantitative DNA detection in a paper-based microfluidic device, 2017.

82. P. H. Rogers, E. Michel, C. A. Bauer, S. Vanderet, D. Hansen, B. K. Roberts, A. Calvez, J. B. Crews, K. O. Lau, A. Wood, D. J. Pine and P. V. Schwartz, "Selective, controllable, and reversible aggregation of polystyrene latex microspheres via DNA hybridization", *Langmuir*, 2005, **21**, 5562.

83. S. A. Opiyo, E. M. Ateka, P. O. Owuor, L. O. A. Manguro and D. W. Miano, "Development of a Multiplex Pcr Technique for Simultaneous Detection of Sweet Potato Feathery Mottle Virus and Sweet Potato Chlorotic Stunt Virus", *Journal of Plant Pathology*, 2010, **92**, 363.